Table 5 Multivariable Cox regression analysis using *PLK1*(log) and dichotomous factors of *β-catenin* mutation, age, stage, and histology ($n = 50$)

Variable	P-*value*	*Variable*	P-*value*	*Variable*	P-*value*
PLK1(log)	0.009	*β-catenin* (mutant vs. wild type)	0.51		
PLK1(log)	0.005	Age (>1 vs ≤1 year)	0.92		
PLK1(log)	0.019	Stage (3, 4 vs 1, 2)	0.46		
PLK1(log)	0.027	Histology (poorly vs well)	0.12		
PLK1(log)	0.052	Histology (poorly vs well)	0.12	Stage (3, 4 vs 1, 2)	0.47

All variables with two categories, except *PLK1*(log)

are downregulated (Table 2). In the library of the latter tumor, *vimentin*, *RNA-binding motif protein*, *Wnt inhibitory factor-1*, *dickkopf*, and *RAP1B* are frequently appeared, whereas they are hardly appeared in the other libraries. Wissmann *et al.* (2003) have recently reported that *WIF1* is downregulated in various cancers (prostate cancer, breast cancer, non-small-cell lung cancer, and bladder cancer), and suggested that loss of WIF1 expression may be an early event in tumorigenesis in those tissues. It is notable that, in contrast to AFP-positive HBLs, the patient's outcome of the tumor with negative AFP is very poor, though the incidence of the latter tumor is low (von Schweinitz *et al.*, 1995). This suggests that AFP-positive and AFP-negative HBLs have a different genetic as well as biological background. In addition, recent reports have demonstrated that frequent mutation of the *β-catenin* gene and nuclear accumulation of its protein product are one of the main causes of the tumorigenesis of HBL. The *APC* and *Axin* genes are also mutated in some HBLs (Oda *et al.*, 1996; Miao *et al.*, 2003; Thomas *et al.*, 2003), indicating that Wnt signaling pathway plays an important role in causing the tumors, most of which are AFP-positive. Therefore, the poor-prognostic HBL without producing AFP might be caused by the particular mechanism additional to or other than the abnormality of Wnt signaling pathway. Although the appearance frequency of the genes in each library does not always reflect the actual expression levels of each gene, it may at least in part show the differences among the tumor subsets with different genetic abnormalities. As our libraries contain many genes involved in liver development, normal liver functions, and carcinogenesis, they must be useful for making a liver-proper cDNA microarray to analyse expression profiles of HBL, viral infection-induced hepatitis, liver cirrhosis, and HCC.

Differentially expressed genes between HBLs and the corresponding normal livers

cDNA microarray, which is often applied to a comprehensive gene expression analysis, is able to detect many genes that are differentially expressed between tumors and normal tissues (Okabe *et al.*, 2001; Nagata *et al.*, 2003). However, it is expensive and needs further confirmation of the selected genes by a semi-quantitative RT–PCR or a real-time RT–PCR method. Therefore, using semi-quantitative RT–PCR and the specific primers of 1188 cDNAs, we have identified 86 genes differentially expressed between HBLs and their corresponding normal livers. Surprisingly, 75 out of 86 genes are preferentially expressed in the latter tissues, and only 11 including *RAN*, *PLK1*, *NPC1*, and *OLR1* known genes are expressed at high levels in HBLs. One of the reasons of this result may be that many gene products, which are necessary for full function in the matured liver metabolism, are dispensable for the malignant growth of the tumor except for the very limited genes. The results of some differentially expressed genes are consistent with those in the previous reports. von Horn *et al.* (2001) have shown that the mRNA levels of *insulin-like growth factor-binding proteins* including *IGFBP-3* are decreased in HBLs than in normal livers. Kinoshita and Miyata (2002) have also reported that *aldolase B* mRNA is downregulated in over 50% of 20 HCCs examined. They proposed that the measurement of aldolase activity in serum is useful to determine the number of collapsed hepatic cells in cirrhosis. Recently, evidences suggest that not only mutant β-catenin but also wild-type β-catenin localize in the cellular nuclei of HBL as well as some other cancers (Rimm *et al.*, 1999; Takayasu *et al.*, 2001). The increased expression of the *Ran* gene in HBLs might be correlated with the shuttling of β-catenin and/or other related proteins between cytoplasm and nucleus in the tumor cells.

Owing to constitutive activation of Wnt signaling in most of the HBLs, the 86 genes differentially expressed between the tumor and its corresponding normal liver were expected to contain downstream target genes of Wnt signaling pathway that might regulate early stage of the hepatic development. In this study, however, only the *lymphocyte alpha-kinase* (*LAK*) gene was found to be differentially expressed at high levels in HBLs with wild-type *β-catenin* and at low levels in those with *β-catenin* mutation. LAK is a new class of protein kinases with a novel catalytic domain, but its precise function is currently unknown (Ryazanov *et al.*, 1999). Thus, our result may suggest that the target genes of the Wnt signaling pathway are commonly affected in HBLs, regardless of the presence or absence of *β-catenin* mutation.

PLK1 as a prognostic indicator of HBL

PLK1 (*polo-like kinase 1*), the human counterpart of *polo* in *Drosophila melanogaster* and of *CDC5* in *Saccharomyces cerevisiae*, encodes a serine/threonine kinase with polo-box domains (Clay *et al.*, 1993). PLK1 is crucial for various events of mitotic progression including centrosome maturation (Lane and Nigg,

1996), spindle function (Glover *et al.*, 1996), activation of cyclin B/Cdc2 (Qian *et al.*, 1998; Toyoshima-Morimoto *et al.*, 2001), and regulation of anaphase-promoting complex (Kotani *et al.*, 1998; Nigg, 1998). Elevated expression of *PLK1* is also found in different types of adult cancers including non-small-cell lung cancer, head and neck tumors, esophageal carcinomas, melanomas, and colorectal cancers (Wolf *et al.*, 1997; Knecht *et al.*, 1999; Tokumitsu *et al.*, 1999; Dietzmann *et al.*, 2001; Takai *et al.*, 2001), implying its critical role in tumorigenesis. In the present study, we have found that *PLK1* is upregulated in primary HBLs, and that its mRNA expression levels are significantly correlated with poor outcome of the patients. Multivariate Cox regression analysis indicated that *PLK1* expression could be an independent prognostic factor from *β-catenin* mutation, age, stage, or histology. However, clinical stage did not show a significant correlation with *PLK1* expression, though it is one of the critical prognostic markers. One of the possible reasons may be that the 59 tumors we used for statistical analysis include two unusual patients, one had stage 4 tumor with good prognosis and another case had stage 1 tumor with poor prognosis. These might have reduced the significance of the tumor stage in patients' survival in our sample set.

It is notable that, among the 1188 genes we have screened for differential expression, *PLK1* is the only one known oncogene overexpressed in the HBL tissues. Smith *et al.* (1997) have reported that constitutive expression of *PLK1* in NIH3T3 cells causes oncogenic focus formation and forms tumors in nude mice. Furthermore, Liu and Erikson (2003) have recently shown that the application of small interfering RNA which specifically depletes *PLK1* expression in cancer cells inhibits cell proliferation, arrests cell cycle, and induces apoptosis. Thus, PLK1 may play a crucial role in causing HBL and other cancers. It may be interesting to examine whether *PLK1* is a target of β-catenin transported from the cytosol into the nucleus. The disruption of PLK1 function could be a future therapeutic tool for the aggressive type of hepatoblastomas.

In conclusion, our HBL cDNA project has provided a large number of genes related to liver development, metabolism, and carcinogenesis. We are currently applying these genes to the cDNA microarray system. Our cDNA resource should be an important tool to understand the molecular mechanism of the genesis of HBL as well as to develop new diagnostic and therapeutic strategies against the aggressive tumors in the future.

Materials and methods

Clinical materials

Tumor tissues and their corresponding normal liver tissues were frozen at the time of surgery and stored at −80°C until use. All specimens were provided from the Tissue Bank of the Japanese Study Group for Pediatric Liver Tumor (JPLT) (Uotani *et al.*, 1998). A total of 74 HBL samples (seven were classified as being stage 1, 17 as stage 2, 26 as stage 3, 15 as stage 4, and nine were unknown stages) were used in this study. The tumors were staged according to the Japanese histopathological classification of HBL (Hata, 1990). From 1991 to 1999, HBLs had been treated by combination chemotherapy using cisplatin and THP-adriamycin according to the JPLT-1 protocol (Sasaki *et al.*, 2002). After 2000, a more intensive chemotherapeutic regimen, ITEC (ifosfamide, THP-adriamycin, etoposide, and carboplatin), has been utilized for tumors that prove resistant to the combination chemotherapy in the JPLT-2 study. Among the 74 tumor samples we examined, 36 and 35 tumor tissues were obtained prior to and after chemotherapy, respectively, and the remaining three were unknown. In the same sample set, 59 tumors were accompanied by outcome information and used for making survival curves, among which 31 and 28 tissues were obtained prior to and after chemotherapy, respectively. Tumor histology was also classified according to Hata (1990). 'Poor histology' indicates 'poorly differentiated (embryonal type)', and 'well histology' indicates 'well-differentiated (fetal type)'. The informed consents were obtained in each institution or hospital. High molecular weight DNA and total RNA of these samples were prepared as described previously (Ichimiya *et al.*, 1999).

Construction of oligo-capping cDNA libraries

Four oligo-capping cDNA libraries, two (HMFT, HYST) derived from HBLs with secretion of AFP, one (HKMT) from HBL without AFP secretion, and one (HMFN) from the corresponding normal liver, were constructed according to the method previously described (Suzuki *et al.*, 1997). These were approved by the institutional review board. The oligo-capping method enables full-length cDNA cloning with high efficiency. The 12 000 cDNA clones in total were randomly picked up and single-run sequencing was performed. Nucleotide sequence of both ends for each cDNA clone was homology-searched against the public nucleotide database using the BLAST program at the National Center for Biotechnology Information (NCBI) (Genbank release 122, January 2001).

Differential screening of the genes by semi-quantitative RT–PCR

The eight samples were selected as PCR templates to screen for the differentially expressed genes. Cases 58 and 81 were defined as stage 2 HBL, cases 10, 67, 78, and 85 were in stage 3, case 14 was in stage 4. Among those eight tumors, four (cases 14, 67, 78, and 81) had the mutant *β-catenin*, and the others (cases 10, 58, 77, and 85) not. Mutation analysis for *β-catenin* was performed as described previously (Takayasu *et al.*, 2001). The differential expression of the genes between the HBL and normal livers was confirmed at least twice using semi-quantitative RT–PCR. The individual gene-specific PCR primer sequences were determined by using Primer3 program (provided at Washington University). For cDNA templates, 5 μg of total RNA was converted to cDNA using random primers (Takara, Otsu, Japan) with SuperScript II RNaseH⁻ reverse transcriptase (Gibco BRL, Rockville, MD, USA). Those cDNAs were at first amplified with *GAPDH* primers for 27 cycles and the amounts of the PCR products were measured by ALF Express™ sequencer and normalized. The amplification was performed 35 or 40 cycles of 95°C for 30 s, 57 or 59 or 61°C for 15 s and 72°C for 60 s, and the final extension was at 72°C for 5 min, using a Perkin-Elmer Thermalcycler 9700 (Perkin-Elmer, Foster City, CA, USA). The PCR products

were run on 2% agarose gels and stained with ethidium bromide. We defined the gene as differentially expressed when it exhibits differential expression between the tumor and its corresponding normal liver in more than four out of the eight samples.

Northern blot analysis

In all, 25 μg of total RNA from the primary HBLs, HCC, and their corresponding normal livers were subjected to Northern analysis. Total RNA was prepared according to the method of Chomczynski and Sacchi (1987). Total RNA was fractionated by electrophoresis on 1% agarose gel containing formaldehyde, transferred onto a nylon membrane filter, and immobilized by UV crosslinking. The hybridization cDNA probe was a 976-base pair human *PLK1* cDNA fragment and labeled with [α-^{32}P]-dCTP using the BcaBEST random priming kit (Takara Biomedicals). The filter was hybridized at 65°C in a solution containing 1 M NaCl, 1% SDS, 7.5% dextran sulfate, 100 μg/ml of heat-denatured salmon sperm DNA, and radiolabeled probe DNA.

Quantitative real-time RT–PCR of PLK1

The primer set for amplification of the *PLK1* and probe sequence are as follows: forward primer, 5′-GCTGCACAAG AGGAGGAAA-3′; reverse primer, 5′-AGCTTGAGGTCTC-GATGAATAAC-3′; probe, 5′-CCTGACTGAGCCTGAGG CCCGATAC-TA-3′. Taqman *GAPDH* control reagents (Perkin-Elmer/Applied Biosystems) were used for the amplification of *GAPDH* as recommended by the manufacturer. PCR was performed using ABI Prism 7700 Sequence Detection System (Perkin-Elmer/Applied Biosystems). In all, 2 μl of cDNA was amplified in a final volume of 25 μl containing 1 × Taqman PCR reaction buffer, 200 μM each dNTP, 0.9 μM each primer, and 200 nM Taqman probe. The optional thermal cycling condition was as follows: 40 cycles of a two-step PCR (95°C for 15 s, 60°C for 60 s) after the initial denaturation (95°C for 10 min). Experiments were carried out in triplicate for each data point.

Statistical analysis

Statistical analyses were performed using Mann–Whitney's *U*-test and Cox regression. A *P*-value of less than 0.05 was considered significant.

Acknowledgements
We are grateful to Shigeru Sakiyama and Toshinori Ozaki for critical reading of the manuscript, and Yoko Nakamura and Aiko Morohashi for experimental support. We thank Eriko Isogai, Naoko Sugimitsu, and Yuki Nakamura for preparing RNA and sequencing analysis, and Natsue Kitabayashi, Emiko Kojima, Emi Goto, and Hisae Murakami for technical assistance. We also thank the hospitals and institutions collaborating with the Japanese Study Group for Pediatric Liver Tumor (JPLT) for providing surgical specimens. This work was supported in part by the fund from Hisamitsu Pharmaceutical Company and a grant-in-aid for Scientific Research on Priority Areas (C) 'Medical Genome Science' from the Ministry of Education, Culture, Sports, Science, and Technology of Japan.

References

Albrecht S, Von Schweinitz D, Waha A, Kraus JA, Von Deimling A and Pietsch T. (1994). *Cancer Res.*, **54,** 5041–5044.
Brady RO, Filling-Katz MR, Barton NW and Pentchev PG. (1989). *Neurol. Clin.*, **7,** 75–88.
Buendia MA. (1992). *Adv. Cancer Res.*, **59,** 167–226.
Buendia MA. (2002). *Med. Pediatr. Oncol.*, **39,** 530–535.
Chomczynski P and Sacchi N. (1987). *Anal. Biochem.*, **162,** 156–159.
Clay FJ, McEwen SJ, Bertoncello I, Wilks AF and Dunn AR. (1993). *Proc. Natl. Acad. Sci. USA*, **90,** 4882–4886.
Dietzmann K, Kirches E, Von Bossanyi, Jachau K and Mawrin C. (2001). *J. Neurooncol.*, **53,** 1–11.
Exelby PR, Filler RM and Grosfeld JL. (1975). *J. Pediatr. Surg.*, **10,** 329–337.
Fukuzawa R, Umezawa A, Ochi K, Urano F, Ikeda H and Hata J. (1999). *Int. J. Cancer*, **82,** 490–497.
Giardiello FM, Petersen GM, Brensinger JD, Luce MC, Cayouette MC, Bacon J, Booker SV and Hamilton SR. (1996). *Gut*, **39,** 867–869.
Glover DM, Ohkura H and Tavares A. (1996). *J. Cell Biol.*, **135,** 1681–1684.
Goldstein JL and Brown MS. (1990). *Nature*, **343,** 425–430.
Gray SG, Eriksson T, Ekstrom C, Holm S, Von Schweinitz D, Kogner P, Sandstedt B, Pietsch T and Ekstrom TJ. (2000). *Br. J. Cancer*, **82,** 1561–1567.
Haas JE, Muczynski KA, Krailo M, Ablin A, Land V, Vietti TJ and Hammond GD. (1989). *Cancer*, **64,** 1082–1095.
Hamanaka R, Kohno K, Seguchi T, Okamura K, Morimoto A, Ono M, Ogata J and Kuwano M. (1992). *J. Biol. Chem.*, **267,** 13160–13165.
Hata Y. (1990). *Jpn. J. Surg.*, **20,** 498–502.
Hata Y, Ishizu H, Ohmori K, Hamada H, Sasaki F, Uchino J, Inoue K, Naitoh H, Fujita M, Kobayashi T and Yokoyama S. (1991). *Cancer*, **68,** 2566–2570.
Hsieh JC, Kodjabachian L, Rebbert ML, Rattner A, Smallwood PM, Samos CH, Nusse R, Dawid IB and Nathans J. (1999). *Nature*, **398,** 431–436.
Ichimiya S, Nimura Y, Kageyama H, Takada N, Sunahara M, Shishikura T, Nakamura Y, Sakiyama S, Seki N, Ohira M, Kaneko Y, McKeon F, Caput D and Nakagawara A. (1999). *Oncogene*, **18,** 1061–1066.
Idilman R, De Maria N, Colantoni A and Van Thiel DH. (1998). *J. Viral. Hepat.*, **5,** 285–299.
Kinoshita M and Miyata M. (2002). *Hepatology*, **36,** 433–438.
Kinzler KW and Vogelstein B. (1996). *Cell*, **87,** 159–170.
Knecht R, Elez R, Oechler M, Solbach C, Von Ilberg C and Strebhardt K. (1999). *Cancer Res.*, **59,** 2794–2797.
Koch A, Denkhaus D, Albrecht S, Leuschner I, Von Schweinitz D and Pietsch T. (1999). *Cancer Res.*, **59,** 269–273.
Kotani S, Tugendreich S, Fujii M, Jorgensen PM, Watanabe N, Hoog C, Hieter P and Todokoro K. (1998). *Mol. Cell*, **1,** 371–380.
Lane HA and Nigg EA. (1996). *J. Cell Biol.*, **135,** 1701–1713.
Li FP, Wendy AT, Seddon J and Holmes GE. (1987). *J. Am. Med. Assoc.*, **257,** 2475–2477.
Li X, Adam G, Cui H, Sandstedt B, Ohlsson R and Ekstrom TJ. (1995). *Oncogene*, **11,** 221–229.
Liu X and Erikson RL. (2003). *Proc. Natl. Acad. Sci. USA*, **100,** 5789–5794.

Loftus SK, Morris JA, Carstea ED, Gu JZ, Cummings C, Brown A, Ellison J, Ohno K, Rosenfeld A, Tagle DA, Pentchev PG and Pavan WJ. (1997). *Science*, **277**, 232–235.

Mann JR, Lakin GE, Leonard JC, Rawlinson HA, Richardson SG, Corkery JJ, Cameron AH and Shah KJ. (1978). *Arch. Dis. Child*, **53**, 366–374.

Miao J, Kusafuka T, Udatsu Y and Okada A. (2003). *Hepatol. Res.*, **25**, 174–179.

Montagna M, Menin C, Chieco-Bianchi L and D'Andrea E. (1994). *J. Cancer Res. Clin. Oncol.*, **120**, 732–736.

Morin PJ, Sparks AB, Korinek V, Barker N, Clevers H, Vogelstein B and Kinzler KW. (1997). *Science*, **275**, 1787–1790.

Nagata T, Takahashi Y, Ishii Y, Asai S, Nishida Y, Murata A, Koshinaga T, Fukuzawa M, Hamazaki M, Asami K, Ito E, Ikeda H, Takamatsu H, Koike K, Kikuta A, Kuroiwa M, Watanabe A, Kosaka Y, Fujita H, Miyake M and Mugishima H. (2003). *Cancer Genet. Cytogenet.*, **145**, 152–160.

Nigg EA. (1998). *Curr. Opin. Cell Biol.*, **10**, 776–783.

Oda H, Nakatsuru Y, Imai Y, Sugimura H and Ishikawa T. (1995). *Int. J. Cancer*, **60**, 786–790.

Oda H, Imai Y, Nakatsuru Y, Hata J and Ishikawa T. (1996). *Cancer Res.*, **56**, 3320–3323.

Okabe H, Satoh S, Kato T, Kitahara O, Yanagawa R, Yamaoka Y, Tsunoda T, Furukawa Y and Nakamura Y. (2001). *Cancer Res.*, **61**, 2129–2137.

Okubo K, Hori N, Matoba R, Niiyama T, Fukushima A, Kojima Y and Matsubara K. (1992). *Nat. Genet.*, **2**, 173–179.

Ortega JA, Krailo MD, Haas JE, King DR, Ablin AR, Quinn JJ, Feusner J, Campbell JR, Lloyd DA, Cherlow J and Hammond GD. (1991). *J. Clin. Oncol.*, **9**, 2167–2176.

Park WS, Oh RR, Park JY, Kim PJ, Shin MS, Lee JH, Kim HS, Lee SH, Kim SY, Park YG, An WG, Kim HS, Jang JJ, Yoo NJ and Lee JY. (2001). *J. Pathol.*, **193**, 483–490.

Polakis P. (1999). *Curr. Opin. Genet. Dev.*, **9**, 15–21.

Qian YW, Erikson E, Li C and Maller JL. (1998). *Mol. Cell. Biol.*, **18**, 4262–4271.

Rainier S, Dobry CJ and Feinberg AP. (1995). *Cancer Res.*, **55**, 1836–1838.

Ribbeck K, Lipowsky G, Kent HM, Stewart M and Gorlich D. (1998). *EMBO J.*, **17**, 6587–6598.

Rimm DL, Caca K, Hu G, Harrison FB and Fearon ER. (1999). *Am. J. Pathol.*, **154**, 325–329.

Ryazanov AG, Pavur KS and Dorovkov MV. (1999). *Curr. Biol.*, **9**, R43–45.

Sasaki F, Matsunaga T, Iwafuchi M, Hayashi Y, Ohkawa H, Ohira M, Okamatsu T, Sugito T, Tsuchida Y, Toyosaka A, Nagahara N, Nishihira H, Hata Y, Uchino J, Misugi K and Ohnuma N. (2002). *J Pediatr Surg.*, **37**, 851–856.

Smith MR, Wilson ML, Hamanaka R, Chase D, Kung H, Longo DL and Ferris DK. (1997). *Biochem. Biophys. Res. Commun.*, **234**, 397–405.

Sudhof TC, Russell DW, Brown MS and Goldstein JL. (1987). *Cell*, **48**, 1061–1069.

Suzuki Y, Yoshitomo-Nakagawa K, Maruyama K, Suyama A and Sugano S. (1997). *Gene*, **200**, 149–156.

Takai N, Miyazaki T, Fujisawa K, Nasu K, Hamanaka R and Miyakawa I. (2001). *Cancer Lett.*, **164**, 41–49.

Takayasu H, Horie H, Hiyama E, Matsunaga T, Hayashi Y, Watanabe Y, Suita S, Kaneko M, Sasaki F, Hashizume K, Ozaki T, Furuuchi K, Tada M, Ohnuma N and Nakagawara A. (2001). *Clin. Cancer Res.*, **7**, 901–908.

Taniguchi K, Roberts LR, Aderca IN, Dong X, Qian C, Murphy LM, Nagorney DM, Burgart LJ, Roche PC, Smith DI, Ross JA and Liu W. (2002). *Oncogene*, **21**, 4863–4871.

Thomas D, Pritchard J, Davidson R, McKiernan P, Grundy RG and de Ville de Goyet J. (2003). *Eur. J. Cancer*, **39**, 2200–2204.

Tokumitsu Y, Mori M, Tanaka S, Akazawa K, Nakano S and Niho Y. (1999). *Int. J. Oncol.*, **15**, 687–692.

Toyoshima-Morimoto F, Taniguchi E, Shinya N, Iwamatsu A and Nishida E. (2001). *Nature*, **410**, 215–220.

Uotani H, Yamashita Y, Masuko Y, Shimoda M, Murakami A, Sakamoto T, Tazawa K and Tsukada K. (1998). *J. Pediatr. Surg.*, **33**, 639–641.

Van Tornout JM, Buckley JD, Quinn JJ, Feusner JH, Krailo MD, King DR, Hammond GD and Ortega JA. (1997). *J. Clin. Oncol.*, **15**, 1190–1197.

Velculescu VE, Vogelstein B and Kinzler KW. (2000). *Trends Genet.*, **16**, 423–425.

Von Horn H, Tally M, Hall K, Eriksson T, Ekstrom TJ and Gray SG. (2001). *Cancer Lett.*, **162**, 253–260.

Von Schweinitz D, Hecker H, Harms D, Bode U, Weinel P, Burger D, Erttmann R and Mildenberger H. (1995). *J. Pediatr. Surg.*, **30**, 845–852.

Von Schweinitz D, Wischmeyer P, Leuschner I, Schmidt D, Wittekind C, Harms D and Mildenberger H. (1994). *Eur. J. Cancer*, **30A**, 1052–1058.

Wang J, Shou J and Chen X. (2000). *Oncogene*, **19**, 1843–1848.

Weber RG, Pietsch T, Von Schweinitz D and Lichter P. (2000). *Am. J. Pathol.*, **157**, 571–578.

Wei Y, Fabre M, Branchereau S, Gauthier F, Perilongo G and Buendia MA. (2000). *Oncogene*, **19**, 498–504.

Weinberg AG and Finegold M. (1983). *Hum. Pathol.*, **14**, 512–537.

Wissmann C, Wild PJ, Kaiser S, Roepcke S, Stoehr R, Woenckhaus M, Kristiansen G, Hsieh JC, Hartmann A, Knuechel R, Rosenthal A and Pilarsky C. (2003). *J. Pathol.*, **201**, 204–212.

Wolf G, Elez R, Doermer A, Holtrich U, Ackermann H, Stutte HJ, Altmannsberger HM, Rubsamen-Waigmann H and Strebhardt K. (1997). *Oncogene*, **14**, 543–549.

Xu XR, Huang J, Xu ZG, Qian BZ, Zhu ZD, Yan Q, Cai T, Zhang X, Xiao HS, Qu J, Liu F, Huang QH, Cheng ZH, Li NG, Du JJ, Hu W, Shen KT, Lu G, Fu G, Zhong M, Xu SH, Gu WY, Huang W, Zhao XT, Hu GX, Gu JR, Chen Z and Han ZG. (2001). *Proc. Natl. Acad. Sci. USA*, **98**, 15089–15094.

Yun K, Jinno Y, Sohda T, Niikawa N and Ikeda T. (1998). *J. Pathol.*, **185**, 91–98.

ELSEVIER

MCN Molecular and Cellular Neuroscience

www.elsevier.com/locate/ymcne
Mol. Cell. Neurosci. 25 (2004) 504–514

Reduced inflammatory pain in mice deficient in the differential screening-selected gene aberrative in neuroblastoma

S. Ohtori,[a,1] E. Isogai,[b,1] F. Hasue,[a] T. Ozaki,[b] Y. Nakamura,[b] A. Nakagawara,[b] H. Koseki,[c] S. Yuasa,[d] E. Hanaoka,[a] J. Shinbo,[a] T. Yamamoto,[e] H. Chiba,[f] M. Yamazaki,[a] H. Moriya,[a] and S. Sakiyama[b,*]

[a] *Department of Orthopaedic Surgery, Graduate School of Medicine, Chiba University, Chuo, Chiba 260-8677, Japan*
[b] *Division of Biochemistry, Chiba Cancer Center Research Institute, Chuo, Chiba 260-8717, Japan*
[c] *Department of Molecular Embryology, Graduate School of Medicine, Chiba University, Chuo, Chiba 260-8677, Japan*
[d] *National Institute of Neuroscience, Kodaira, Tokyo 187-8502, Japan*
[e] *Department of Anaesthesiology, Graduate School of Medicine, Chiba University, Chuo, Chiba 260-8677, Japan*
[f] *Third Department of Anatomy, Graduate School of Medicine, Chiba University, Chuo, Chiba 260-8677, Japan*

Received 10 February 2003; revised 21 November 2003; accepted 1 December 2003

Differential screening-selected gene aberrative in neuroblastoma (Dan) protein is produced in small neurons of dorsal root ganglia. Thermal and mechanical allodynia and Fos expression in the spinal dorsal horn evoked by inflammation and neuropathic pain were investigated using Dan-deficient mice. Mice showed pain reactions induced by the introduction of complete Freund's adjuvant (CFA) into their hind paw (inflammatory pain model) and after sciatic nerve ligation (neuropathic pain model). In the inflammatory pain model, thermal and mechanical pain thresholds in Dan-deficient mice were significantly higher than those of wild-type mice. The number of Fos-immunoreactive cells in the dorsal horn during the inflammatory period was significantly less in Dan-deficient mice. However, in the neuropathic pain model, no differences in thermal hypersensitivity, mechanical allodynia, or the number of Fos-immunoreactive cells in the dorsal horn were observed between the mice. These data suggest that Dan may be a neuromodulator in inflammatory pain.

Introduction

The differential screening-selected gene aberrative in neuroblastoma (*Dan*) was initially cloned as an mRNA down-regulated in v-*src*-transformed rat fibroblasts (Ozaki and Sakiyama, 1993). The analysis of *Dan* function by transfection of cultured cells revealed that *Dan* has an ability to suppress the transformed phenotype and delay entry into the S phase, suggesting that *Dan* carries a tumor-suppressive activity (Ozaki and Sakiyama, 1994; Ozaki et al., 1995). Recently, it has been shown that *Dan* is a founding member of a novel gene family that includes the *Xenopus* head-inducing factor, *Cerberus* and the dorsalizing factor, *Gremlin* (Hsu et al., 1998). *Dan* family members play crucial roles in early mouse embryonic development by inhibiting the signaling derived from bone morphogenetic proteins (BMPs) as well as modulating the action of transforming growth factor β (TGF-β) superfamily members (Hsu et al., 1998; Pearce et al., 1999; Piccolo et al., 1999; Stanley et al., 1998). Dionne et al. (2001) showed that Dan-deficient mice displayed subtle and background-dependent defects, suggesting that functional redundancy exists among *Dan* family members.

We previously showed the existence of Dan in primary small-diameter sensory nerve fibers, and also demonstrated that Dan mediates inflammatory pain, but not pain due to nerve injury (Ohtori et al., 2002). However, the precise mechanism underlying this action is unknown. In the present study, we have produced Dan-deficient mice and investigated inflammation and nerve injury-evoked thermal and mechanical allodynia and Fos expression in the spinal dorsal horn of Dan-deficient and wild-type mice.

Results and discussion

Generation of Dan-deficient mice

Mice with disrupted *Dan* alleles were generated using homologous recombination in embryonic stem cells to replace exons II and III with a neomycin-resistant gene (Fig. 1A). Genotyping of mutant mice was performed by Southern blot (Fig. 1B) and PCR (Fig. 1C) analyses using the probes and primers, respectively, as indicated in Fig. 1A. *Dan* mRNA was expressed in several organs in wild-type mice; however, as expected, it was not detected in Dan-deficient mice (Fig. 1D). Dionne et al. (2001) reported that Dan-deficient mice do not show apparent defects. In the current study, Dan-deficient mice did not show obvious differences when compared with wild-type mice during development, infancy, and adulthood. In the central and peripheral nervous systems, there were no morphologic changes in the Dan-deficient mice.

* Corresponding author. Division of Biochemistry, Chiba Cancer Center Research Institute, 666-2 Nitona, Chuo, Chiba 260-8717, Japan. Fax: +81-43-265-4459.
E-mail address: ssakiyam@chiba-cc.pref.chiba.jp (S. Sakiyama).
[1] These authors have contributed equally to this work.
Available online on ScienceDirect (www.sciencedirect.com.)

1044-7431/$ - see front matter © 2004 Elsevier Inc. All rights reserved.
doi:10.1016/j.mcn.2003.12.002

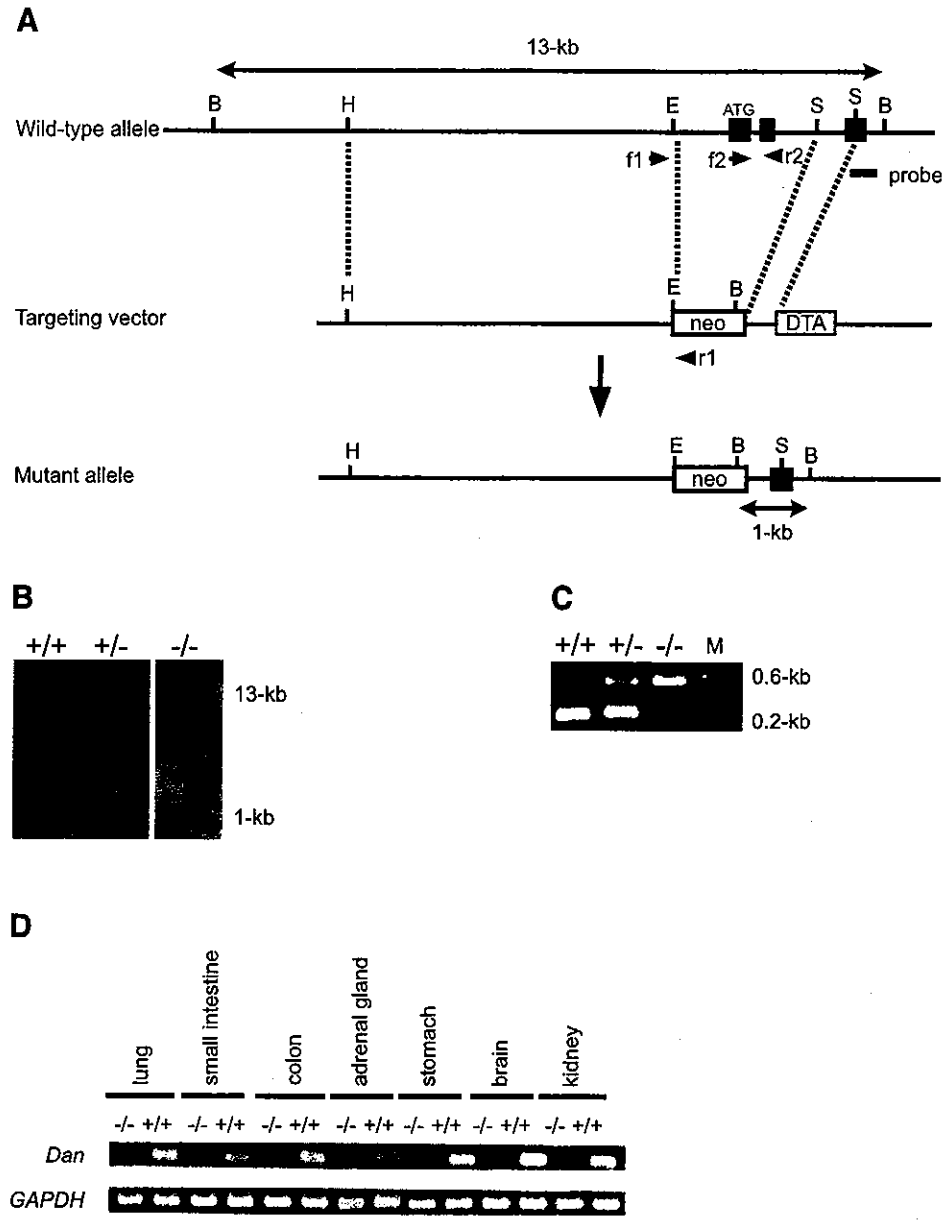

Fig. 1. Generation of Dan-deficient mice. (A) Schematic drawing of gene targeting strategy. The map of the wild-type *Dan* allele spans the region between intron I and exon IV (top). Filled boxes indicate the exons II, III, and IV. The targeting vector (middle) was constructed as described in the Experimental methods. Arrowheads indicate the locations of PCR primers used for detecting the wild-type or mutant allele: forward-1 (f1) and reverse-1 (r1) for the mutant allele, and forward-2 (f2) and reverse-2 (r2) for the wild-type allele. The location of the probe (0.4-kb *Sma*I–*Xba*I restriction fragment) used for Southern analysis is indicated by the solid bar. This probe detects 13- and 1-kb fragments derived from the wild-type and the mutant alleles, respectively. The mutant allele is shown below the targeting vector. B, *Bam*HI; H, *Hin*cII; E, *Eco*RI; S, *Sma*I. (B) Southern blot analysis of tail DNA from wild-type (+/+), heterozygous (+/−), and homozygous (−/−) mutant mice. Genomic DNA was digested with *Bam*HI, transferred to a nylon membrane, and hybridized with the external probe shown in A. The positions of migration of the fragments derived from wild-type (13 kb) and disrupted alleles (1 kb) are indicated. (C) PCR analysis of tail DNA from wild-type (+/+), heterozygous (+/−), and homozygous (−/−) mutant mice. PCR products were separated on a 2% agarose gel by electrophoresis and visualized by ethidium bromide staining. The positions of migration of the fragments derived from wild-type (0.2 kb) and disrupted alleles (0.6 kb) are indicated. M, DNA molecular weight marker. (D) RT-PCR analysis of *Dan* expression in wild-type (+/+) and homozygous (−/−) mutant mice. Total RNA was prepared from the indicated adult mouse organs and subjected to RT-PCR using specific primers for *Dan* or *GAPDH*. Amplification of *GAPDH* was used as an internal control.

SP, CGRP, NK1, and Dan in the primary sensory neurons under physiological conditions

Double-staining for Dan with CGRP, IB4, P2X3, or NF200

SP- and CGRP-IR neurons were observed in the DRG of both wild-type and Dan-deficient mice (Fig. 2). These neurons were small to intermediate in size. We found that 69 ± 7% (mean ± SE) of all DRG neurons were Dan-IR in wild-type mice, whereas none of DRG neurons were Dan-IR in Dan-deficient mice ($P < 0.01$). The distributions and percentages of SP- and CGRP-IR DRG neurons were not significantly different between wild-type and Dan-deficient mice (wild-type, SP: 26 ± 4%, CGRP, 38 ± 6%;

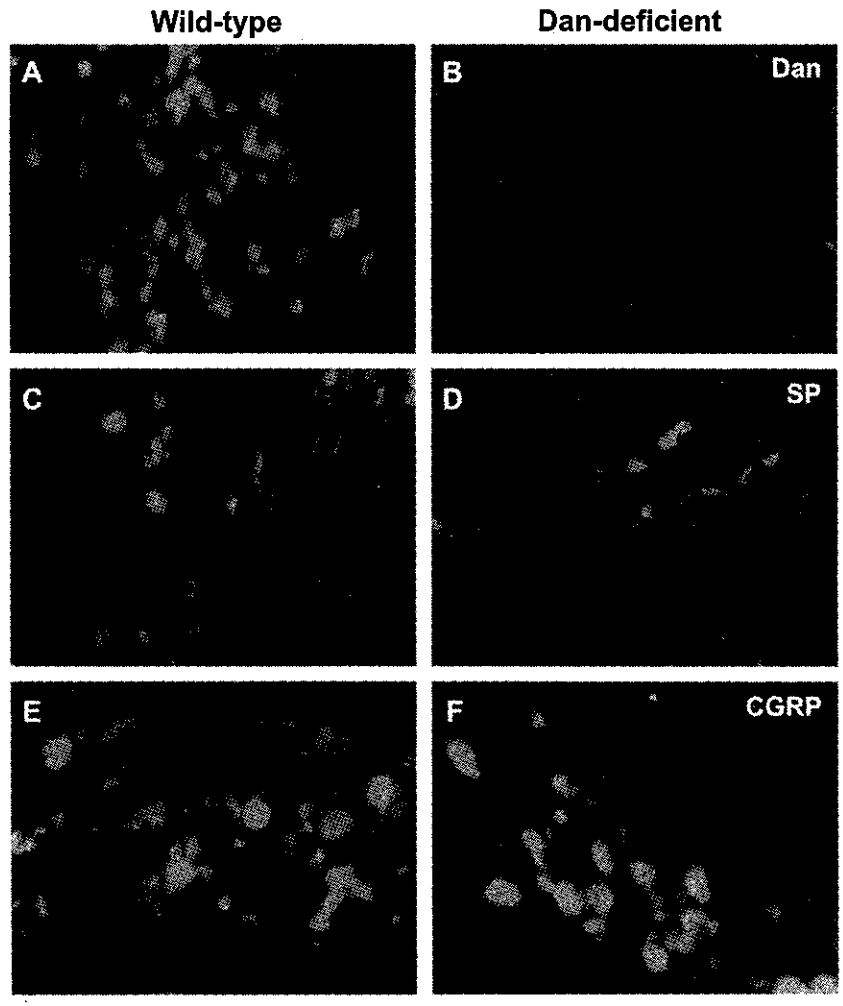

Fig. 2. Dan was absent in DRG neurons of Dan-deficient mice (B). DRG neurons derived from wild-type (A, C, and E) and Dan-deficient mice (B, D, and F) were reacted with antibody to Dan (A and B), substance P (SP) (C and D), or calcitonin gene-related peptide (CGRP) (E and F).

Dan-deficient, SP: 23 ± 5%; CGRP, 42 ± 7%) (mean ± SE) ($P > 0.1$). In the spinal dorsal horn of wild-type mice, Dan-IR sensory nerve terminals were observed in the inner part of lamina II, and SP- and CGRP-IR sensory nerve terminals were observed in laminae I and II (Fig. 3). NK1-IR neurons were detected mainly in laminae I and III. The patterns of SP-, CGRP-, and NK1-IR terminals in the spinal dorsal horn were not significantly different between wild-type and Dan-deficient mice.

Dan-IR nerve fibers were observed where a dorsal root lesion was made in wild-type mice (Fig. 3). Dan-IR free nerve endings were observed in the dermis of the footpads of wild-type mice, but not detectable in the skin of the footpads of Dan-deficient mice (Fig. 3). Two weeks after spinal nerve root section, the number of Dan-IR nerve terminals in the spinal dorsal horn decreased in wild-type mice. Because *Dan* mRNA was expressed in small DRG neurons (Ohtori et al., 2002), Dan was produced in small DRG neurons and seemed to be transported into the spinal dorsal horn and skin of footpads.

Dan immunoreactivity was seen in CGRP-, IB4-, and P2X3-IR neurons (Fig. 4). In all of the Dan-IR neurons, the ratios of Dan-IR neurons labeled with CGRP, IB4, or P2X3 were 33 ± 3%, 55 ± 9%, or 64 ± 8% (mean ± SE), respectively. On the other hand, some Dan was co-localized with NF200-IR myelinated A-fiber neurons (12 ± 3%). The ratios of Dan-IR neurons also labeled with CGRP, IB4, or P2X3 were significantly higher than that of neurons labeled with NF-200-IR ($P < 0.01$). Most of the double-labeled neurons were small-sized A-fiber neurons (Fig. 4).

Interestingly, Dan-IR nerve terminals in the spinal dorsal horn were located only in the inner part of lamina II. Interneurons in the inner part of lamina II differ considerably from those located dorsally in lamina I and in the outer part of lamina II. Immunocytochemical studies of the localization of the P2X3 receptor indicated its presence in a subpopulation of small-diameter non-peptidergic neurons that specifically bind IB4; these neurons project to (the inner part of) lamina II in the dorsal horn (Bradbury et al., 1998; Llewellyn-Smith and Burnstock, 1998). Dan-positive small DRG neurons stained with IB4 and P2X3 could project into the inner part of lamina II.

Almost all of the small DRG neurons were Dan-IR. In comparison, it has been reported that, respectively, only 20% and about 40% of small DRG neurons are substance P- and CGRP-containing (Neumann et al., 1996). In the current study, CGRP-IR DRG neurons were double-labeled with Dan. Non-IB4 and P2X3-IR Dan-positive DRG neurons were SP- or CGRP-containing small neurons projecting into lamina I and the outer layer of lamina II. However, it is unclear why Dan immunoreactivity in the spinal

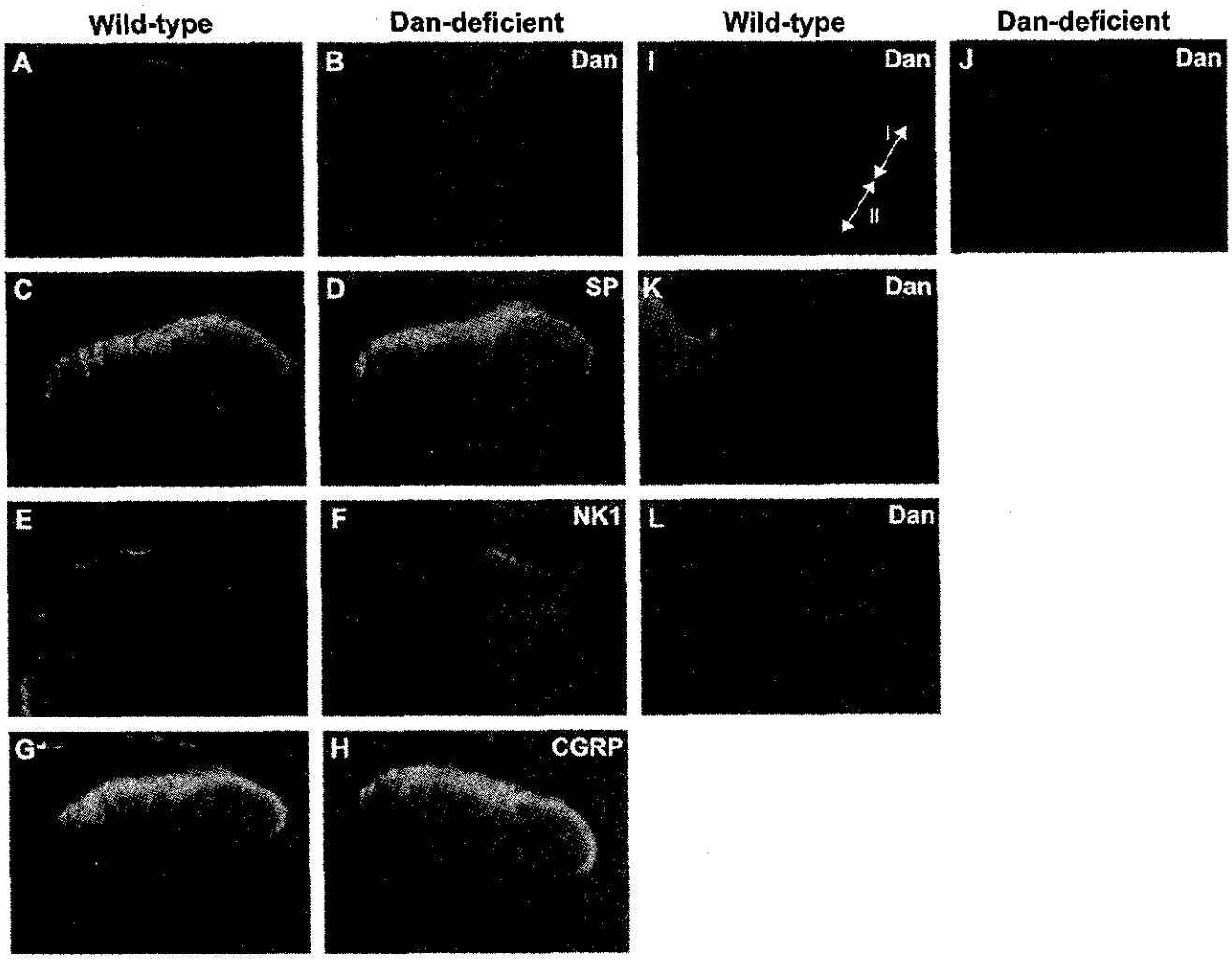

Fig. 3. In wild-type mice, DAN-IR sensory nerve terminals were observed in the inner part of lamina II, whereas Dan was absent in the spinal dorsal horn of Dan-deficient mice (B). In both types of mice, SP- (C and D) and CGRP-IR (G and H) sensory nerve terminals were detected in laminae I and II. Neurokinin receptor (NK1)-IR neurons were observed mainly in laminae I and III (E and F). Dan-IR sensory nerve endings in the dermis of footpads and sensory nerves in spinal dorsal root lesion were seen in wild-type mice (I and K), whereas they were not observed in the footpads of Dan-deficient mice (J). I, Epidermis; II, Dermis. Dan-IR nerve terminals in spinal dorsal horn decreased 2 weeks after dorsal root cut (L).

dorsal horn is seen only in the inner part of lamina II. One possible reason is that Dan protein in peptidergic neurons may not be transported to the central terminals in the spinal cord.

It has been reported that specific TGF-β family members are candidate regulators of CGRP expression in embryonic sensory neurons. BMPs 2, 4, and 6 stimulated CGRP expression in 60% of DRG neurons. BMP4 application supported maximal CGRP induction, suggesting that BMP4 is a "switch" rather than a continuous modulator of neuropeptide phenotype (Ai et al., 1999). In our study, we did not observe any differences in the distributions and ratios of SP- and CGRP-IR DRG neurons and sensory terminals in the spinal dorsal horn under physiological conditions. Dan seems not to regulate CGRP expression in embryonic and adult sensory neurons.

Thermal hypersensitivity and mechanical allodynia after inflammation

In the absence of inflammation or nerve injury, we found no differences in paw withdrawal responses to thermal and mechanical stimulation between Dan-deficient and wild-type mice. In wild-type and Dan-deficient mice, CFA injection produced a significant reduction in paw withdrawal latency to a heat stimulus on the injected side ($P < 0.01$) (Fig. 5A). Also, both types of mice displayed a significant mechanical allodynia ($P < 0.01$) (Fig. 5B). However, this decrease in the threshold of thermal and mechanical allodynia in Dan-deficient mice was significantly less than that of wild-type mice ($^*P < 0.05$). Injury to the sciatic nerve produced a significant decrease in the paw withdrawal threshold to thermal and von Frey hair stimulation on the injured side of wild-type ($P < 0.01$) and Dan-deficient mice ($P < 0.01$); however, the decrease in threshold between the two groups was not significantly different ($P > 0.1$) (Figs. 5C and D).

We previously showed that the Dan protein in rat DRG neurons increased only following CFA injection, but did not change following partial nerve injury. Furthermore, intrathecal injection of an antibody to Dan suppressed only inflammatory pain caused by the introduction of CFA and it did not suppress pain due to nerve injury (Ohtori et al., 2002).

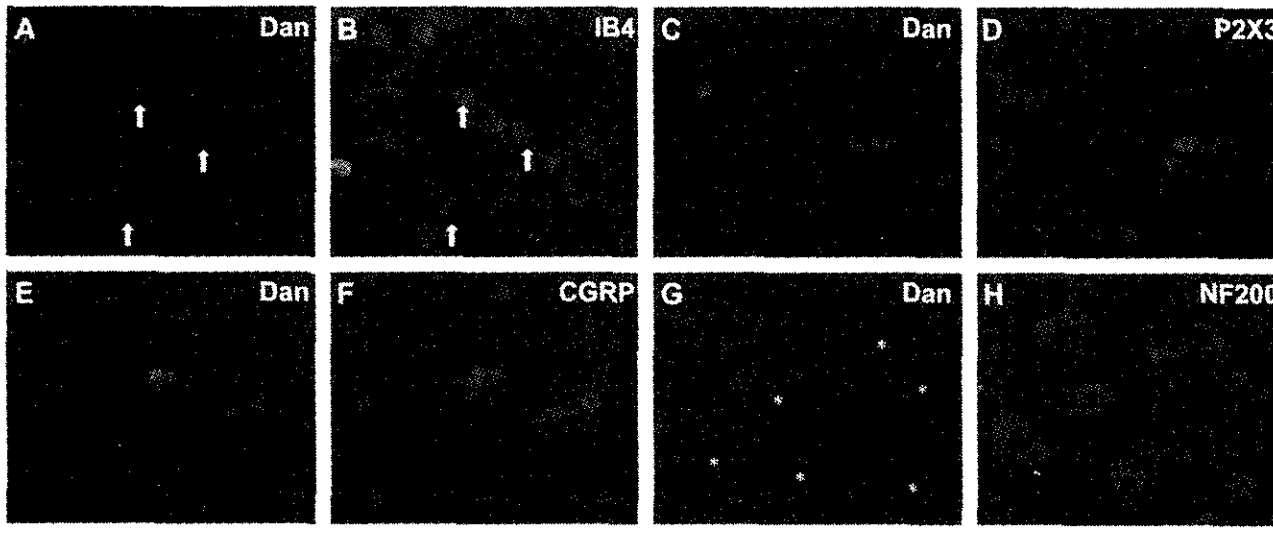

Fig. 4. Micrographs showing double-staining for Dan with isolectin B4 (IB4) (A and B), P2X3 (C and D), CGRP (E and F), or neurofilament 200 (NF200) (G and H). Dan was double-labeled with CGRP-IR DRG neurons. Dan immunoreactivity was seen in most IB4 and P2X3-IR neurons. On the other hand, most of Dan was not double-labeled in NF200-IR myelinated A-fiber neurons. Asterisks indicate Dan-IR and NF200-negative neurons.

It has also been reported that, in inflammatory models, SP and CGRP were increased in the dorsal root ganglia and the dorsal horn of the lumbar spinal cord (Donnerer et al., 1992; Noguchi and Ruda, 1992; Noguchi et al., 1988) and that the neurokinin receptor (NK1) was increased in the dorsal horn (Abbadie et al., 1996; McCarson and Krause, 1994).

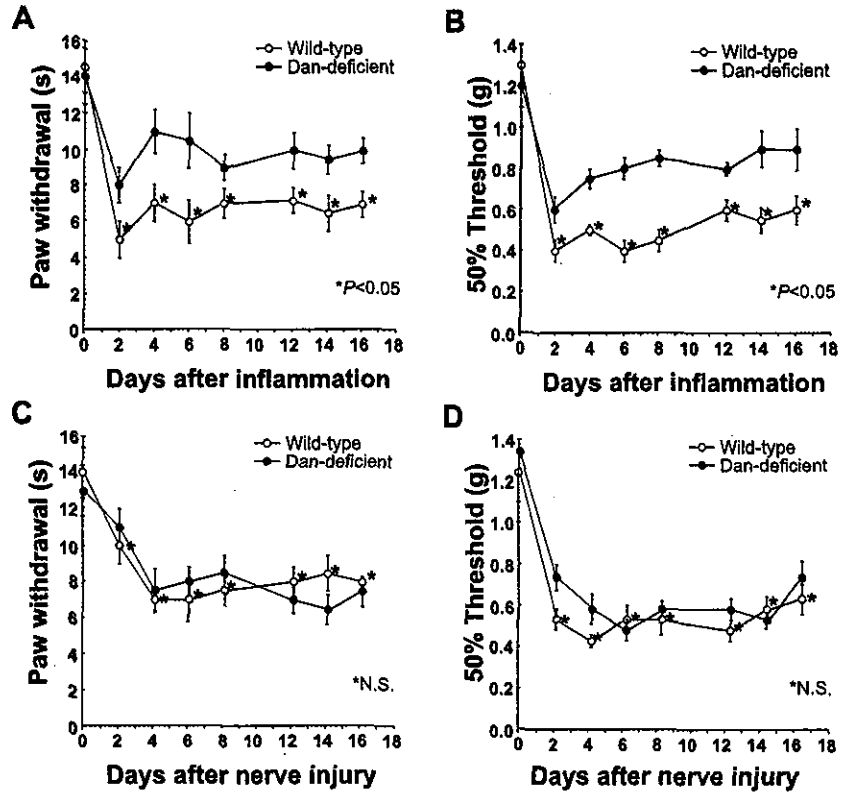

Fig. 5. Hyperalgesia measured by withdrawal to noxious thermal stimulation of the hind paw (A). The data are expressed as the difference in paw withdrawal latency between wild-type and Dan-deficient mice. After injection of CFA, significant reduction in paw withdrawal latency was observed in both types of mice; however, the decrease was significantly different between wild-type and Dan-deficient mice ($P < 0.05$). Inflammation also produced a significant decrease in paw withdrawal threshold (B). Asterisks indicate a significantly lower threshold on the inflammatory side in the wild-type mice compared with that of Dan-deficient mice ($P < 0.05$). Nerve injury also produced hyperalgesia measured by withdrawal to noxious thermal stimulation of the hind paw (C) and a significant decrease in the paw withdrawal threshold to von Frey filament stimulation (D). However, there were no differences between wild-type and Dan-deficient mice ($P > 0.1$).

Indeed, 4 days after inflammation in the current study, the fractions of SP- and CGRP-IR DRG neurons were 40 ± 4% (mean ± SE) and 52 ± 5%, respectively, in wild type and corresponding values for Dan-deficient mice were 31 ± 4% and 49 ± 5% (Figs. 6 and 7). The ratio of SP- and CGRP-IR neurons in both types of mice significantly increased compared with a non-inflammatory control ($P < 0.05$). The ratio of SP-IR neurons in wild-type mice was higher than that in Dan-deficient mice ($P < 0.05$) (Figs. 6 and 7); however, there was no significant difference in the ratio of CGRP-IR neurons in both types of mice after inflammation ($P > 0.1$). The relationship between Dan and other peptides influenced by neuropathic or inflammatory pain remains unclear. It is possible that Dan might induce SP in DRG neurons under inflammatory conditions.

Protein kinase C gamma (PKC) staining is also confined to interneurons of the inner part of lamina II. Mice that lack PKC displayed normal responses to acute pain stimuli, but they almost completely failed to develop a neuropathic pain syndrome after partial sciatic nerve section (Malmberg et al., 1997). On the other hand, the P2X3 receptor is important during inflammatory periods and may play a role in the modulation of spinal nociceptive transmission following the development of inflammation, but these receptors play at most a minor role in spinal nociceptive processing in normal and neuropathic animals (Liu and Tracey, 2000; Stanfa et al., 2000). Dan, which was expressed in the inner part of lamina II, seems to regulate only inflammatory pain.

Depression of Fos expression in inflammatory pain

Fos-IR neurons were present mainly in the left dorsal horn (Figs. 8 and 9). The time course of Fos expression following CFA injection in wild-type and Dan-deficient mice is shown in Fig. 10. The numbers of Fos-IR neurons following CFA injection in the superficial and deep laminae of Dan-deficient mice were significantly less than those in wild-type mice ($P < 0.05$) (Fig. 11A). The amount of Fos expression in lamina II of Dan-deficient mice was significantly less than that in wild-type mice ($P < 0.05$) (Fig. 11C). The difference was detected for all the periods we observed

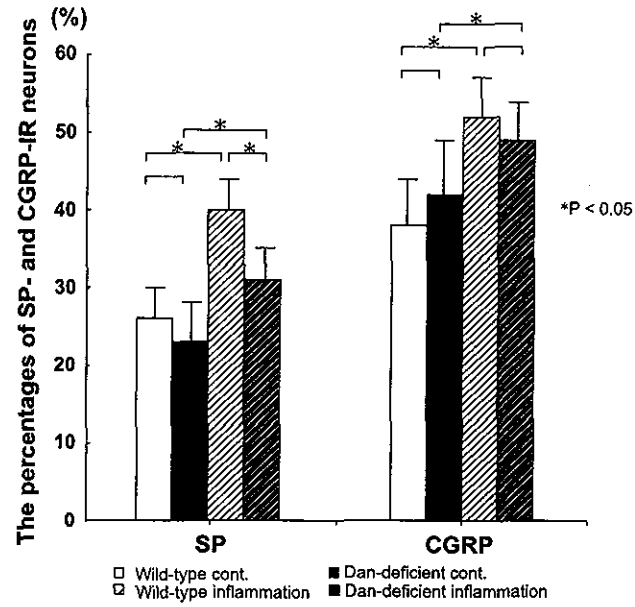

Fig. 7. The percentages of SP- and CGRP-IR DRG neurons were not significantly different between wild-type and Dan-deficient mice under normal conditions (day 0; wild type, SP: 26 ± 4%, CGRP, 38 ± 6%; Dan-deficient, SP: 23 ± 5%, CGRP, 42 ± 7%) (mean ± SE) ($P > 0.1$). Four days after inflammation, the ratios of SP- and CGRP-IR neurons in both types of mice were significantly increased compared with non-inflammatory control ($P < 0.05$). The ratio of SP-IR neurons in wild-type mice was higher than that in Dan-deficient mice ($P < 0.05$). However, there was no significant difference in the ratio of CGRP-IR neurons in both types of mice after inflammation ($P > 0.1$).

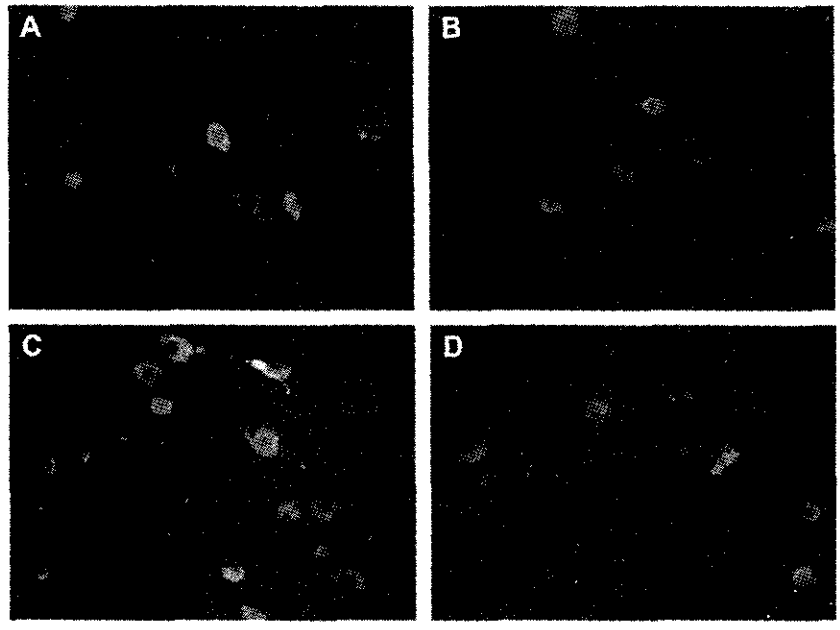

Fig. 6. Change in ratio of SP-IR DRG neurons of wild type (A, control group; C, inflammatory group) and Dan-deficient (B, control group; D, inflammatory group) mice after inflammation. SP was increased in wild-type and Dan-deficient mice after inflammation (C and D), however the number of SP-IR DRG neurons in wild-type mice (C) was significantly higher than that in Dan-deficient mice (D).

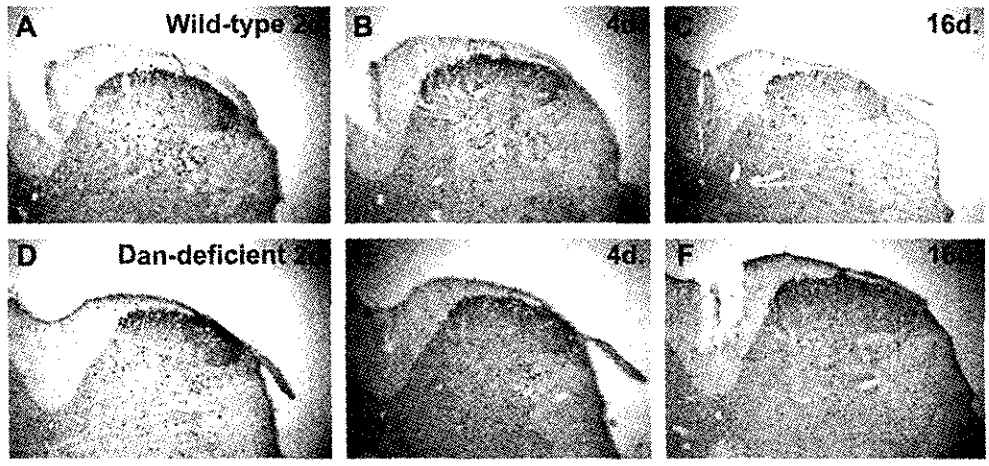

Fig. 8. Inflammation-induced Fos expression in the spinal dorsal horn in wild-type (A, B, and C) and Dan-deficient mice (D, E, and F). Fos-IR neurons in the superficial and deep laminae were observed at days 2 (A and D), 4 (B and E), and 16 (C and F) after CFA injection into the hind paw. More neurons were stained in wild-type mice than in Dan-deficient mice.

(Fig. 11). The amount of Fos expression in lamina I and II, 4 days after inflammation, was depressed by intrathecal injection of Dan antibody in wild-type mice ($P < 0.05$) (Figs. 10 and 11D). However, in the partial nerve injury models, the numbers of Fos-IR neurons following nerve injury in the superficial and deep laminae of Dan-deficient mice were not significantly different from those in wild-type mice ($P > 0.1$) (Fig. 11B).

It has been reported that noxious chemical and thermal stimulation of the skin leads to Fos expression in spinal dorsal horn neurons (Hunt et al., 1987). An increase of Fos expression in the spinal cord is observed following nerve injury in animal models (Catheline et al., 1999; Chi et al., 1993; Dai et al., 2001; Hudspith et al., 1999). The increase of Fos in the superficial and deep laminae may be related to hypersensitivity to noxious and innocuous stimuli following nerve injury (Catheline et al., 1999; Dai et al., 2001). After inflammation of the rat hind paw, noxious and innocuous stimuli induced a significantly large increase in Fos expression by dorsal horn neurons in laminae I–VI during lasting peripheral inflammation (Ma and Woolf, 1996).

In the current study, Fos expression was observed in superficial and deep laminae in the inflammatory and nerve injury models. We observed the same pattern, period, and location of spinal dorsal horn Fos expression as previously reported. Dan-deficient mice did not show significant hypersensitivity and mechanical allodynia caused by inflammation when compared with wild-type mice. However, the Dan-deficient mice showed hypersensitivity and mechanical allodynia caused by nerve injury. This finding was correlated with the decreased Fos expression observed in Dan-deficient mice under inflammatory conditions and with an insignificant difference in Fos expression after nerve injury when compared with wild-type mice.

Because Dan-IR nerve terminals were in the inner part of lamina II, the localization of Dan may lead to depression of Fos expression only in the inner part of lamina II in Dan-deficient mice. However, Fos expression was decreased in all superficial and deep laminae in the spinal dorsal horn. We postulate that the reason for this is as follows: it has been reported that NK1 receptor-immunoreactive neurons with cell bodies in lamina III or IV and dendrites that enter the superficial laminae also receive dense synaptic innervation from SP primary afferents (Todd et al., 2002). After inflammation of rat hind paw, Fos expression is more common in neurons with NK1 receptors. Therefore, a significant

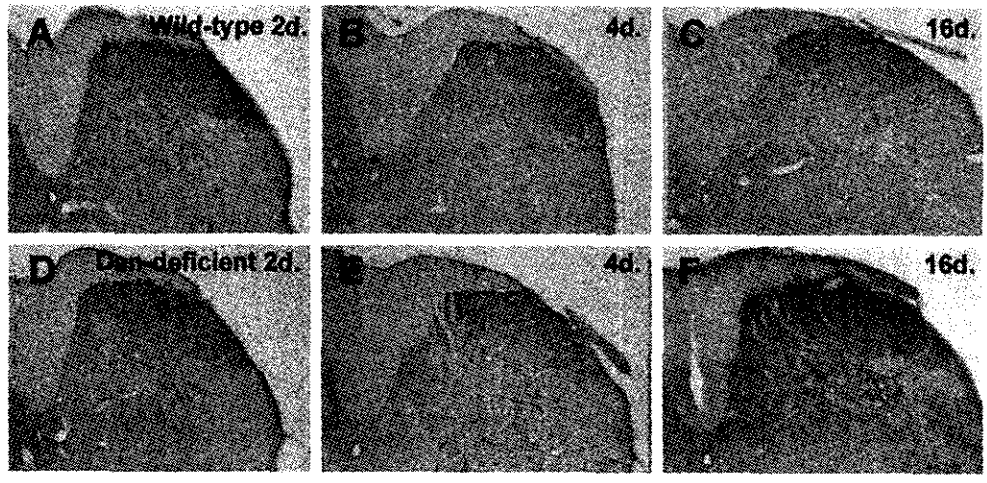

Fig. 9. Fos expression after nerve ligation in the spinal dorsal horn in wild-type (A, B, and C) and Dan-deficient mice (D, E, and F). The number of Fos-IR neurons at days 2 (A and D), 4 (B and E), and 16 (C and F) after nerve ligation was not significantly different between wild-type and Dan-deficient mice.

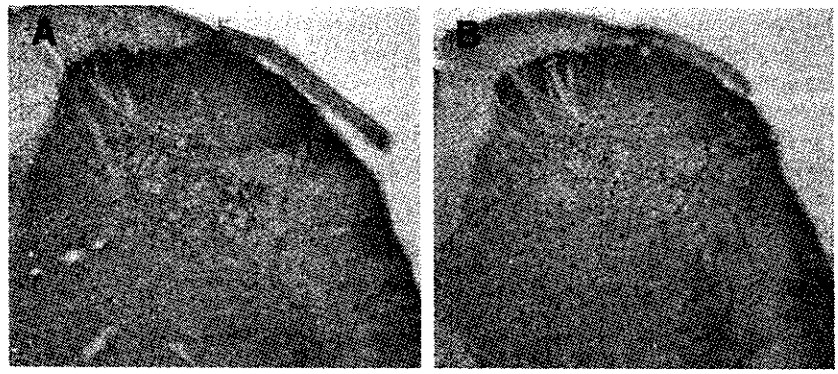

Fig. 10. Effect of intrathecally administered Dan monoclonal antibody on a CFA model of wild-type mice 4 days after inflammation. The level of Fos expression in superficial and deep layers 2 h after stimulation was depressed by intrathecal injection of Dan antibody in wild-type mice. (A, administration of mouse IgG; B, administration of Dan antibody).

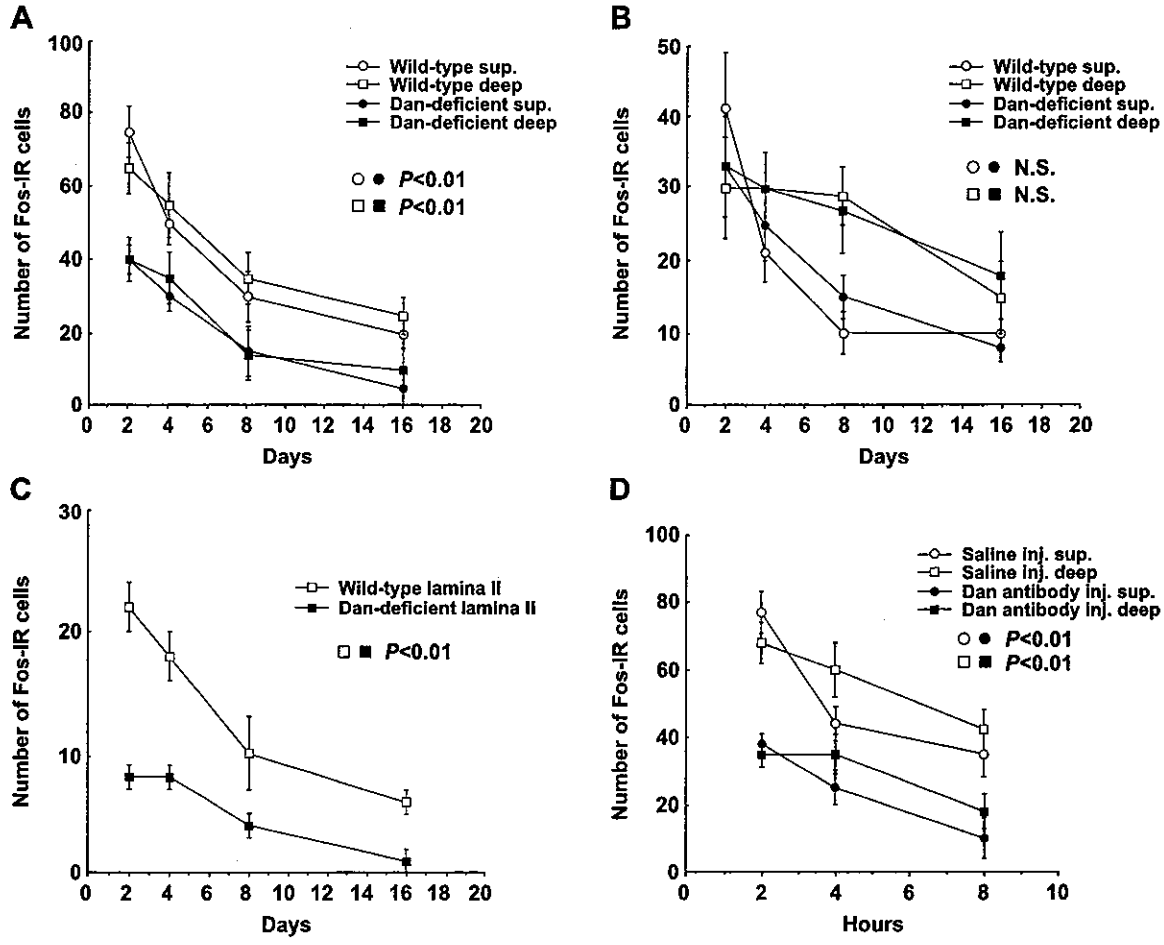

Fig. 11. Time course of Fos expression caused by inflammation in wild-type (open symbols) and Dan-deficient mice (solid symbols) (A). The numbers of Fos-IR cells in both laminae were less in Dan-deficient mice than in wild-type mice at all periods we observed ($P < 0.01$). In lamina II, immunoreacted for Dan, the number of Fos-IR cells was less in Dan-deficient mice (open square) than in wild-type mice (solid square) ($P < 0.01$) (C). Stimulation of the hind paw produced Fos in wild-type and Dan-deficient mice after nerve injury (B). On days 2, 4, 8, and 16, we did not observe significant differences in the numbers of Fos-IR cells in the superficial and deep laminae between both types of mice (open circle, wild-type superficial; open square, wild-type deep; solid circle, Dan-deficient superficial; solid square, Dan-deficient deep) ($P > 0.1$). The amount of Fos expression in superficial and deep layers 4 days after inflammation was depressed by intrathecal injection of Dan antibody in wild-type mice ($P < 0.05$) (Fig. 8D). Each point represents the time after stimulation of footpads (open circle, Fos expression in the superficial layers after IgG administration; open square, Fos expression in the deep layers after IgG administration; solid circle, Fos expression in the superficial layers after Dan-antibody administration; solid square, Fos expression in the deep layers after Dan-antibody administration).

proportion of these cell bodies in deep layers would be excited by noxious stimulation (Todd et al., 2002). SP was increased in the dorsal root ganglia, and the amount of these peptides in projections from the dorsal horn of the lumbar spinal cord would also be increased in inflammatory models (Schaible et al., 1994; Neumann et al., 1996; Noguchi et al., 1995). In the process, Dan is related to SP induction in DRG neurons after inflammation in the current study. We did not examine Dan receptors in the spinal cord. However, intrathecal-administered Dan suppressed pain behavior and Fos expression in superficial and deep layers of the spinal cord. We therefore propose that, except for SP induction in DRG, Dan also stimulates Fos in Dan-immunoreactive cells in the deep layer via the Dan-receptor pathway.

Experimental methods

The protocols for animal procedures in these experiments followed National Institutes of Health guidelines for the Care and Use of Laboratory Animals (1996 revision) and received approval from the ethics committees of our institutions.

Generation of Dan-deficient mice

A radio-labeled full-length mouse *Dan* cDNA was used to screen a mouse genomic library (λFIXII) by standard procedures. Genomic clones that gave a positive signal in the initial screening were digested with various combinations of restriction enzymes to verify that rearrangements had not occurred. The targeting construct was generated by replacing a 2.5-kb *Eco*RI–*Sma*I restriction fragment containing the exons II and III with an MC1-Neo cassette. An MC1-DT-A cassette was then inserted into the 3′ side of the Neo cassette for negative selection. Forty micrograms of the linearized targeting vector were electroporated into 6×10^6 R1 ES cells, and the transfected cells were maintained in the presence of G418. Genomic DNA was prepared from the G418-resistant clones and subjected to Southern analysis using a radiolabeled *Sma*I–*Xba*I restriction fragment as a probe. Of 240 clones analyzed, two clones carried the desired mutant allele. These two targeted ES cell clones were then injected into BDF1 blastocysts to generate chimeric mice. Chimeras were mated with C57BL/6 females and lines were maintained by backcross onto C57BL/6 females.

Genotyping of mice at the Dan locus

Animals were genotyped either by Southern blot hybridization or by PCR-based analysis. For Southern analysis, mouse genomic DNA was digested completely with *Bam*HI, separated by 0.8% agarose gel electrophoresis, and transferred onto a nylon membrane filter. The filter was probed with the radiolabeled *Sma*I–*Xba*I restriction fragment. This strategy identified a 13-kb wild-type allele or a 1-kb targeted allele. PCR analysis was performed with the following primers: forward-1 (f1), 5′-ATACCTGCTTCCCCACTCCT-3′, reverse-1 (r1), 5′-GAACCTGCGTGCAATCCATCTT-3′; and forward-2 (f2), 5′-GACAAGAGTGCCTGGTGTGA-3′, reverse-2 (r2), 5′-GTGTTGGGGACGCTGTAACT-3′, which resulted in a 458-bp mutant type and a 227-bp wild-type product, respectively. The cycling conditions were 2 min at 98°C and 35 cycles of 30 s at 98°C, 30 s at 62°C, and 30 s at 72°C.

Inflammation model and nerve injury model

Forty-eight 12-week-old male Dan-deficient and wild-type mice were used. Under anesthesia with sodium pentobarbital (40 mg/kg, ip), 20 μl of complete Freund's adjuvant (CFA; 50 μg *Mycobacterium butyricum* in an oil-in-saline emulsion; Sigma, St. Louis, MO) was injected into the left hind paw. Partial sciatic nerve injury was caused by tight ligation of one-third to one-half of the left sciatic nerve.

Behavioral testing

The latency of paw withdrawal to thermal stimuli was measured as has been previously described (Hargreaves et al., 1988). Wild-type and Dan-deficient mice were placed in a planter test apparatus (UGO Basile; Camerio, Italy) consisting of a radiant heat source below an elevated floor of transparent glass. The radiant heat source beneath the glass floor was turned on, and the time between the start of stimulation and hind paw withdrawal was measured five times every 10 min. The average time for hind paw withdrawal was recorded. The level of tactile allodynia was estimated from 50% probability thresholds for paw withdrawal from mechanical stimuli using von Frey hairs, as previously described (Chaplan et al., 1994).

Time course of Fos expression in CFA and nerve injury models

Touch-evoked increases in Fos expression were examined from 2 to 16 days after CFA injection or nerve injury to wild-type (n = 24) and Dan-deficient mice (n = 24). Gentle touch stimuli were applied manually to the injected plantar surface of these animals with the flat surface of the experimenter's thumb, as described in detail previously (Sivilotti and Woolf, 1994). Each touch, lasting 2 s and moving from the middle position of the foot to the distal footpad, was applied once every 4 s for 10 min under halothane anesthesia.

We examined the effect of intrathecally administered mouse monoclonal antibody to Dan (5 μg) (Chiba Cancer Center Research Institute) on the CFA model in wild-type mice 4 days after inflammation (n = 12). To administer antibodies intrathecally, a 30-gauge needle was inserted into the intralamina space between L6 and S1. Stimulation of the footpad was applied after intrathecal injection of Dan antibody. To obtain control data, 5 μg of mouse IgG_1 was administered (n = 12). The number of Fos-immunoreactive (IR) cells in the spinal cord was evaluated 2, 4, and 8 h after stimulation.

Immunohistochemistry

Mice were anesthetized with 3% halothane and perfused transcardially with 100 ml of 4% paraformaldehyde (PFA) in phosphate buffer (0.1 M, pH 7.4). The spinal cord was resected at the level of C4 and L5, and the L5 dorsal root ganglia (DRGs) and footpad were removed and 20-μm sections cut on a cryostat. To examine axonal transport of Dan from DRG to the spinal dorsal horn, the spinal cord at the level of L4 was resected 2 weeks after dorsal root section. Sections were incubated in a blocking solution containing 0.3% Triton X-100 and 5% skim milk in 0.01 M phosphate-buffered saline (PBS) for 90 min at room temperature. Sections were processed immunohistochemically using a free-floating avidin–biotin complex (ABC) technique by incubating them with rabbit antibody to Dan (1:1000 in blocking solution), substance P

(SP) (1:100; Zymed, San Francisco, CA), calcitonin gene-related protein (CGRP) (1:2000; Chemicon, Temecula, CA), neurokinin receptor (NK1) (Dr. R. Shigemoto, Kyoto University, Japan), or Fos (1:1000; Santa Cruz Biotechnology, Santa Cruz, CA) for 20 h at 4 °C, followed by incubation with biotinylated goat anti-rabbit IgG (Vector Labs, Burlingame, CA; 1:100 in blocking solution) and fluorescein isothiocyanate (FITC) avidin D (1:100; Vector Labs). For Fos immunostaining of the spinal cord, after incubation with an avidin–biotin enzyme complex (Vector Labs; 1:100 in blocking solution) for 90 min at room temperature, immunoreaction was visualized using an ammonium nickel sulfate enhanced diaminobenzidine (DAB) reaction. We counted cells in 7 serial sections of the DRG and 10 sections of the spinal cord. The number of Dan-, SP-, and CGRP-IR neurons in the DRG, and Fos-IR neurons in the laminae I, II, and those in the deep layers (laminae III–VI) were counted.

Double-labeling immunohistochemistry

After incubation with rabbit antibody to Dan for 20 h at 4 °C, sections were incubated with goat anti-rabbit Alexa 488 (FITC) (1:400; Molecular Probes Inc., Eugene, OR).

Sections were incubated with mouse antibody to CGRP (marker for peptergic small neurons; 1:2000; Chemicon, Temecula, CA), isolection B4 (IB4; marker for non-peptidergic small neurons; 1:1000; Chemicon, Temecula, CA), guinea pig antibody to P2X3 (marker for non-peptidergic small neurons; 1:2000; Neuromic, Minneapolis, MN), or mouse antibody to neurofilament 200 (NF200; marker for myelinated A fiber s neurons; 1:1000; Chemicon, Temecula, CA) for 20 h at 4 °C CGRP, isolectin B4, P2X3 and NF200 were visualized by following incubation with goat anti-mouse Alexa 594 (Texas red; 1:400), streptavidin Alexa 594 (Texas red; 1:400), goat anti-guinea pig Alexa 594 (Texas red; 1:400), and goat anti-mouse Alexa 594 (Texas red; 1:400), respectively.

Statistical analysis

The differences among the groups were compared using ANOVA. Differences were considered to be statistically significant at $P < 0.05$.

Acknowledgments

We thank Dr. R. Shigemoto (Kyoto University) for the gift of antibody to NK1 and K. Kitajo for technical assistance.

References

Abbadie, C., Brown, J.L., Mantyh, P.W., Basbaum, A.I., 1996. Spinal cord substance P receptor immunoreactivity increases in both inflammatory and nerve injury models of persistent pain. Neuroscience 70, 201–209.

Ai, X., Cappuzzello, J., Hall, A.K., 1999. Activin and bone morphogenetic proteins induce calcitonin gene-related peptide in embryonic sensory neurons in vitro. Mol. Cell. Neurosci. 14, 506–518.

Bradbury, E.J., Burnstock, G., McMahon, S.B., 1998. The expression of P2X3 purinoreceptors in sensory neurons: effects of axotomy and glial-derived neurotrophic factor. Mol. Cell. Neurosci. 12, 256–268.

Catheline, G., Le Guen, S., Honore, P., Besson, J.M., 1999. Are there long-term changes in the basal or evoked Fos expression in the dorsal horn of the spinal cord of the mononeuropathic rat? Pain 80, 347–357.

Chaplan, S.R., Bach, F.W., Pogrel, J.W., Chung, J.M., Yaksh, T.L., 1994. Quantitative assessment of tactile allodynia in the rat paw. J. Neurosci. Methods 53, 55–63.

Chi, S.I., Levine, J.D., Basbaum, A.I., 1993. Effects of injury discharge on the persistent expression of spinal cord *fos*-like immunoreactivity produced by sciatic nerve transection in the rat. Brain Res. 617, 220–224.

Dai, Y., Iwata, K., Kondo, E., Morimoto, T., Noguchi, K., 2001. A selective increase in Fos expression in spinal dorsal horn neurons following graded thermal stimulation in rats with experimental mononeuropathy. Pain 90, 287–296.

Dionne, M.S., Skarnes, W.C., Harland, R.M., 2001. Mutation and analysis of Dan, the founding member of the Dan family of transforming growth factor beta antagonists. Mol. Cell. Biol. 21, 636–643.

Donnerer, J., Schuligo, I.R., Stein, C., 1992. Increased content and transport of substance P and calcitonin gene-related peptide in sensory nerves innervating inflamed tissue: evidence for a regulatory function of nerve growth factor in vivo. Neuroscience 49, 693–698.

Hargreaves, K., Dubner, R., Brown, F., Flores, C., Joris, J., 1988. A new and sensitive method for measuring thermal nociception in cutaneous hyperalgesia. Pain 32, 77–88.

Hudspith, M.J., Harrisson, S., Smith, G., Bountra, C., Elliot, P.J., Birch, P.J., Hunt, S.P., Munglani, R., 1999. Effect of post-injury NMDA antagonist treatment on long-term *fos* expression and hyperalgesia in a model of chronic neuropathic pain. Brain Res. 822, 220–227.

Hsu, D.R., Economides, A.N., Wang, X., Eimon, P.M., Harland, R.M., 1998. The *Xenopus* dorsalizing factor Gremlin identifies a novel family of secreted proteins that antagonize BMP activities. Mol. Cell 1, 673–683.

Hunt, S.P., Pini, A., Evan, G., 1987. Induction of c-*fos*-like protein in spinal cord neurons following sensory stimulation. Nature 328, 632–634.

Liu, T., Tracey, D.J., 2000. ATP P2X receptors play little role in the maintenance of neuropathic hyperalgesia. NeuroReport 11, 1669–1672.

Llewellyn-Smith, I.J., Burnstock, G., 1998. Ultrastructural localization of P2X3 receptors in rat sensory neurons. NeuroReport 9, 2545–2550.

Ma, Q.P., Woolf, C.J., 1996. Basal and touch-evoked *fos*-like immunoreactivity during experimental inflammation in the rat. Pain 67, 307–316.

Malmberg, A.B., Chen, C., Tonegawa, S., Basbaum, A.I., 1997. Preserved acute pain and reduced neuropathic pain in mice lacking PKCgamma. Science 278, 279–283.

McCarson, K., Krause, J.E., 1994. NK-1 and NK-3 type tachykinin receptor mRNA expression in the rat spinal cord dorsal horn is increased during adjuvant or formalin induced nociception. J. Neurosci. 14, 712–720.

Neumann, S., Doubell, T.P., Leslie, T., Woolf, C.J., 1996. Inflammatory pain hypersensitivity mediated by phenotypic switch in myelinated primary sensory neurons. Nature 384, 360–364.

Noguchi, K., Ruda, M.A., 1992. Gene regulation in an ascending nociceptive pathway: inflammation-induced increase in preprotachykinin mRNA in rat lamina I spinal projection neurons. J. Neurosci. 12, 2563–2572.

Noguchi, K., Kawai, Y., Fukuoka, T., Senba, E., Miki, K., 1995. Substance P induced by peripheral nerve injury in primary afferent sensory neurons and its effect on dorsal column nucleus neurons. J. Neurosci. 11, 7633–7643.

Noguchi, K., Morita, Y., Kiyama, H., Ono, K., Tohyama, M., 1988. A noxious stimulus induces the preprotachykinin-A gene expression in the rat dorsal root ganglion: a quantitative study using in situ hybridization histochemistry. Brain Res. 464, 31–35.

Ohtori, S., Yamamoto, T., Ino, H., Hanaoka, E., Shinbo, J., Ozaki, T., Takada, N., Nakamura, Y., Chiba, T., Nakagawara, A., Sakiyama, S., Sakashita, Y., Takahashi, K., Tanaka, K., Yamagata, M., Yamazaki, M., Shimizu, S., Moriya, H., 2002. Differential screening-selected gene aberrative in neuroblastoma protein modulates inflammatory pain in the spinal dorsal horn. Neuroscience 110, 579–586.

Ozaki, T., Sakiyama, S., 1993. Molecular cloning and characterization of a cDNA showing negative regulation in v-*src*-transformed 3Y1 rat fibroblasts. Proc. Natl. Acad. Sci. U. S. A. 90, 2593–2597.

Ozaki, T., Sakiyama, S., 1994. Tumor-suppressive activity of N03 gene product in v-*src*-transformed rat 3Y1 fibroblasts. Cancer Res. 54, 646–648.

Ozaki, T., Nakamura, Y., Enomoto, H., HilRose, M., Sakiyama, S., 1995. Overexpression of DAN gene product in normal rat fibroblasts causes a retardation of the entry into the S phase. *Cancer Res.* 55, 895–900.

Pearce, J.J., Penny, G., Rossant, J., 1999. A mouse cerberus/Dan-related gene family. Dev. Biol. 209, 98–110.

Piccolo, S., Agius, E., Leyns, L., Bhattacharyya, S., Grunz, H., Bouwmeester, T., De Robertis, E.M., 1999. The head inducer Cerberus is a multifunctional antagonist of Nodal. BMP and Wnt signals. Nature 397, 707–710.

Schaible, H.G., Freudenberger, U., Neugebauer, V., Stiller, R.U., 1994. Intraspinal release of immunoreactive calcitonin gene-related peptide during development of inflammation in the joint in vivo-a study with antibody microprobes in cat and rat. Neuroscience 62, 1293–1305.

Sivilotti, L., Woolf, C.J., 1994. The contribution of GABAA and glycine receptors to central sensitization: disinhibition and touch-evoked allodynia in the spinal cord. J. Neurophysiol. 72, 169–179.

Stanfa, L.C., Kontinen, V.K., Dickenson, A.H., 2000. Effects of spinally administered P2X receptor agonists and antagonists on the responses of dorsal horn neurones recorded in normal, carrageenan-inflamed and neuropathic rats. Br. J. Pharmacol. 129, 351–359.

Stanley, E., Biben, C., Kotecha, S., Fabri, L., Tajbakhsh, S., Wang, C.C., Hatzistavrou, T., Roberts, B., Drinkwater, C., Lah, M., Buckingham, M., Hilton, D., Nash, A., Mohun, T., Harvey, R.P., 1998. DAN is a secreted glycoprotein related to *Xenopus* cerberus. Mech. Dev. 77, 173–184.

Todd, A.J., Puskar, Z., Spike, R.C., Hughes, C., Watt, C., Forrest, L., 2002. Projection neurons in lamina I of rat spinal cord with the neurokinin 1 receptor are selectively innervated by substance P-containing afferents and respond to noxious stimulation. J. Neurosci. 22, 4103–4113.

Identification of novel human neuronal leucine-rich repeat (h*NLRR*) family genes and inverse association of expression of *Nbla10449/*h*NLRR-1* and *Nbla10677/*h*NLRR-3* with the prognosis of primary neuroblastomas

SHIHO HAMANO[1,2], MIKI OHIRA[1], ERIKO ISOGAI[1], KOUNOSUKE NAKADA[2] and AKIRA NAKAGAWARA[1]

[1]Division of Biochemistry, Chiba Cancer Center Research Institute, 666-2 Nitona, Chuoh-ku, Chiba 260-8717; [2]Division of Pediatric Surgery, St. Marianna University School of Medicine, 2-16-1 Sugao, Miyamae-ku, Kawasaki 216-8511, Japan

Received August 1, 2003; Accepted September 24, 2003

Abstract. To search for novel prognostic indicators, we previously cloned >2,000 novel genes from primary neuroblastoma (NBL) cDNA libraries and screened for differential expression between the subsets with favorable (stage 1 or 2 with a single copy of *MYCN*) and unfavorable (stage 3 or 4 with amplification of *MYCN*) prognosis. From them, we have identified 3 genes of human neuronal leucine-rich repeat protein (NLRR) family: *Nbla10449/*h*NLRR-1*, *Nbla00061/*h*NLRR-2/GAC1* and *Nbla10677/*h*NLRR-3*. An additional family member, h*NLRR-5*, was also found by homology search against public database. NLRR family proteins have been proposed to function as a neuronal adhesion molecule or soluble ligand binding receptor like *Drosophila toll* and *slit* with multiple domains including 11 sets of extracellular leucine-rich repeat (LRR)-motifs. However, the functional role of the NLRR protein family has been elusive. Our present study shows that h*NLRR* mRNAs are preferentially expressed in nervous system and/or adrenal gland. In cancer cell lines, h*NLRR-1*, h*NLRR-3* and h*NLRR-5* are expressed at high levels in the neural crest-derived cells. Most remarkably, in primary NBLs, h*NLRR-1* is significantly expressed at high levels in unfavorable subsets as compared to favorable ones, whereas the expression pattern of h*NLRR-3* and h*NLRR-5* is the opposite. In order to understand the function of these receptors, we have used newborn mouse superior cervical ganglion (SCG) cells which are dependent on nerve growth factor (NGF) for their survival. Expression of the mouse counterparts of h*NLRR-2* and h*NLRR-3* is up-regulated after NGF-induced differentiation and down-regulated after NGF depletion-induced apoptosis. On the other hand, expression of h*NLRR-1* and h*NLRR-5* is inversely regulated in the same system. These results have suggested that the regulation of the h*NLRR* family genes may be associated with NGF signaling pathway in both SCG cells and neuroblastoma. Our quantitative real-time RT-PCR analysis using 99 primary NBLs has revealed that high levels of h*NLRR-1* expression are significantly associated with older age (>1 year, p=0.0001), advanced stages (p=0.0007), low expression of *TrkA* (p=0.011), and *MYCN* amplification (p=0.0001), while those of h*NLRR-3* expression are significantly correlated with the favorable prognostic indicators. Furthermore, multivariate analysis reveals that expression of h*NLRR-1* is an independent prognostic indicator in human neuroblastoma. Thus, our results demonstrate that, despite being members of the same family, h*NLRR-1* and h*NLRR-3* may share different biological function among the NBL subsets, and that their expression level becomes novel prognostic indicators of NBL.

Correspondence to: Dr Akira Nakagawara, Division of Biochemistry, Chiba Cancer Center Research Institute, 666-2 Nitona, Chuoh-ku, Chiba 260-8717, Japan
E-mail: akiranak@chiba-ccri.chuo.chiba.jp

Key words: leucine-rich repeat, neuroblastoma, differential expression, prognostic factor

Introduction

Neuroblastoma (NBL) is one of the most common pediatric tumors originating from sympathoadrenal lineage of the neural crest. NBL shows variable biological behavior which characterizes different clinical subsets (1). The tumors found in young children, <1 year of age usually regress spontaneously, while those in the older children are often aggressive leading to poor outcome. Recent advances in molecular biology have identified the important molecules involved in the regulation of growth, differentiation and programmed cell death during development of the sympathoadrenal cells (2), some of which link to the modulation of NBL biology. These include Trk family tyrosine kinase receptors and *MYCN* proto-oncogene. TrkA, a high-affinity receptor for nerve growth factor (NGF), is expressed in favorable subsets of NBL and regulates differentiation and/or regression of the tumor cells (3). On the other hand, TrkB, a receptor for brain-derived neurotrophic factor (BDNF) and neurotrophin-4 (NT-4), is expressed in NBLs with unfavorable prognosis. An autocrine loop of BDNF/NT-4 and TrkB may promote tumor cell survival and increase their invasiveness (4). Amplification of *MYCN* is significantly associated with allelic loss of the

distal region of chromosome 1, and both are indicators of poor prognosis. A recent report suggests that *MYCN* oncoprotein induces expression of *Id-2* with a helix-loop-helix domain and in turn negatively regulates Rb tumor suppressor in NBL (5). However, many important genes may still be missing for better understanding of NBL biology as well as predicting the prognosis. In order to identify novel NBL-related genes and promote better understanding of the molecular mechanism of NBL genesis and its biology, differential screening method has been applied (6).

We have previously constructed full-length-enriched oligocapping cDNA libraries from different subsets of primary NBL (6,7). One derived from the mixture of favorable NBLs in stage 1 with single-copy of *MYCN*, and the other from unfavorable NBLs in stage 3 and 4 with *MYCN* amplification. We have finished end-sequencing of 2,500 clones obtained from each library, and found that the expression profile is markedly different between the subsets. So far, 1,800 independent genes from these libraries have been subjected to semi-quantitative RT-PCR using 16 favorable and 16 unfavorable NBLs to find the genes differentially expressed between favorable (F) and unfavorable (UF) subsets (8,9).

In this study, we have identified novel human *NLRR* family genes that are differentially expressed among the NBL subsets. NLRRs are proteins with leucine-rich repeat (LRR) domains which may be involved in protein-protein interactions (10). They may also function as cell-adhesion molecules or signaling receptors implicated in regulation of the neural development. Expression of the h*NLRR-1/Nbla10449* gene is significantly associated with short survival as well as conventional poor-prognostic factors, whereas that of the h*NLRR-3/Nbla10677* gene is increased in favorable subset of NBL. Our results suggest that the differential expression of h*NLRR* genes among the NBL subsets is involved in the regulation of growth, differentiation and cell death of human NBL.

Materials and methods

Patients. We studied tumors from 99 children with NBL diagnosed between 1995-1999. Fifty-four Japanese patients were identified by a mass screening program started in 1985 (9,10). The selection of tumors for this study was solely based on the availability of a sufficient amount of tumor tissue, from which DNA and mRNA could be prepared for the analyses described below.

The diagnosis of NBL was confirmed by histologic assessment of the tumor specimen obtained at surgery according to the classification of Shimada *et al* (11). There were 57 tumors with favorable histology, and 42 with unfavorable histology. The tumors were staged according to the International Neuroblastoma Staging System (INSS) (12). Thirty-eight tumors (36 identified by mass screening) were stage 1, 14 (11 identified by mass screening) stage 2, 5 (3 identified by mass screening) stage 4s, 10 (3 identified by mass screening) stage 3, and 32 (1 identified by mass screening) stage 4. The patients were treated according to the protocols previously described (13).

Tumor samples and cell lines. Fresh, frozen tumorous tissues were sent to the Division of Biochemistry, Chiba Cancer Center Research Institute, from various hospitals in Japan with informed consent from the patient's parents. All samples were obtained by surgery (or biopsy) and stored at -80°C. Studies were approved by the Institutional Review Board of the Chiba Cancer Center. Human cell lines which we used included NBL (CHP134, CHP*901*, GANB, GOTO, IMR32, SMS-KAN, SMS-KCN, KP-N-NS, LAN-5, NB-1, NB-9, NBKM-1, NB (Tu)-1, NLF, NMB, RTBM1, SMS-SAN, SK-N-BE, SK-N-DZ, TNB, TGW, LHN, NGP, NB69, NBL-S, OAN, SK-N-AS, SK-N-SH, SH-SY5Y, and CNB-RT), osteosarcoma (OST, Saos2, and NOS1), rhabdomyosarcoma (RMS-MK and ASPS-KY), colorectal adenocarcinoma (COLO320, SW480, and LOVO), a hepatocellular cancer (HepG2), breast cancer (MOA-MB-453 and MB231), melanoma (G361, G32TG, A875), a thyroid cancer (TTC11), a gastric cancer (KATO3), esophageal cancer (ECGI10), a pancreatic cancer (ASPC1) and a lung cancer cell lines (A549). The cells were cultured in the RPMI-1640 medium (Nissui Pharmaceutical Co. Ltd., Tokyo) with 10% fetal bovine serum and 50 μg/ml penicillin/streptomycin at humidified 5% CO_2/95% air at 37°C.

Primary culture of newborn mouse superior cervical ganglion cells. The SCG neurons were isolated from newborn mice, and treated with 50 ng/ml of NGF for 5 days, as previously reported (14). RNAs were isolated 12, 24, and 48 h after depleting NGF and adding anti-NGF antibody (1% v/v).

Northern blot analysis. Multiple Tissue Northern blot purchased from Clontech (Palo Alto, CA, USA) was used for Northern analysis with cDNA fragments labeled with α-[^{32}P]dCTP as probes. Hybridization was performed in the ExpressHyb hybridization buffer (Clontech) at 68°C for 1 h. Membrane was washed twice in 2X SSC/0.05% SDS at room temperature for 30 min, twice in 0.1X SSC/0.1% SDS at 50°C for 40 min. After washing, the filter was autoradiographed with X-ray film. The membrane was boiled in 0.1% SDS for 10 min for reprobing, and rehybridized with ß-actin as a control.

Semi-quantitative RT-PCR. cDNA was synthesized from 5 μg of total RNA in a 20 μl reaction mixture containing 200 units of Superscript II reverse transcriptase (Life Technologies, Inc.) and pd$(N)_6$ random hexamer (Takara Shuzo Co., Ltd., Ohtsu, Japan). The resulting cDNA fragments were diluted to be a 1:10 solution for PCR templates. The following pairs of forward and reverse primer sets were prepared for amplification: *NLRR-1*, 5'-GTCGATGTCCATGAATACAAC CT-3' and 5'-CAAGGCTAATGACGGCAAAC-3'; *NLRR-2*, 5'-TGACCTATTCCTGACGG-3' and 5'-AAATCACAGTCT CGGGC-3'; *NLRR-3*, 5'-ACTCTTGCCTAATACCCTGAC-3' and 5'-AGATGGTATTCGAGCACTTTG-3'; *GAPDH*, 5'-CTGCACCAACAATATCCC-3' and 5'-GTAGAGACA GGGTTTCAC-3'. All PCR amplifications were performed with a Perkin-Elmer Corp. GeneAmp PCR 9700, using rTaq polymerase (Takara Shuzo Co., Ltd.) with 35 cycles of sequential denaturation (95°C for 15 sec) and annealing-extension (58°C for 15 sec and 72°C for 1 min). *GAPDH* was used as a control and amplified under the same condition except for reduced amplification cycles to 28. PCR templates

were standardized by its *GAPDH* expression before performing semi-quantitative PCR. The products were electrophoresed on 2.0% agarose gels and stained with ethdium bromide for visualization.

Quantitative real-time RT-PCR. cDNA was prepared by the same method as in the semi-quantitative RT-PCR and 2 µl of the 40-fold dilution was used for each PCR reaction. Primers and TaqMan probes for *Nbla10449* and *Nbla10677* were designed using the primer design software Primer Express™ (Perkin-Elmer Applied Biosystems). TaqMan GAPDH control reagent kit (Perkin-Elmer Applied Biosystems) was used for *GAPDH* expression as a control. Reaction mixture (25 µl), containing 2 µl of cDNA, 1X TaqMan mixture, 0.3 µM forward and reverse primers, and 0.2 µM TaqMan probe were used for PCR. The condition of PCR was as follows: 2 min at 50°C (stage 1), 10 min at 95°C (stage 2), and then 50 cycles of amplification for 15 sec at 95°C and 1 min at 60°C (stage 3).

Statistical analysis. The student's t-tests were used to explore possible associations between *Nbla10449/hNLRR-1* expression and other factors, such as age. Since the values of the *Nbla10449/hNLRR-1* and *Nbla10677/hNLRR-3* expression were skewed, a log transformation was used to achieve the normality when using t-test and Cox regression. The distinction between high and low levels of *Nbla10449* was based on the median value (low, *Nbla10449* <0.31 d.u.; high, Nbla10449 >0.31 d.u.), regardless of tumor stage, *MYCN* copy number, or survival. The distinction between high and low levels of *Nbla10677* was based on the median value (low, *Nbla10677* <1.04 d.u.; high, *Nbla10677*>1.04 d.u.), regardless of tumor stage, *MYCN* copy number, or survival. Kaplan-Meier survival curves were calculated, and survival distributions were compared using the log-rank test. Cox regression models were used to explore associations between *Nbla10449/Nbla10677*, age, *MYCN* copy number, mass screening, tumor origin and survival. Statistical significance was declared if the p value was <0.05. Statistical analysis was performed using Stata 6.0. (Stata Statistical Software: Release 6.0 College Station, Stata Corporation, TX, 1999).

Results

Identification of novel human homologues of NLRR family genes, Nbla10449/hNLRR-1 and Nbla10677/hNLRR-3, and their differential expression between favorable and unfavorable subsets of neuroblastoma. To identify the genes differentially expressed between favorable and unfavorable NBLs, semi-quantitative RT-PCR analyses were performed. Sixteen favorable (F) and 16 unfavorable (UF) NBLs were used as PCR templates after normalization by GAPDH expression. So far, ~1,800 independent genes from the NBL cDNA libraries have been surveyed, resulting in the approximately 300 genes with differential expression between the subsets (8,9). Among them, we found *Nbla10449* and *Nbla10677* genes that are highly homologous to the mouse *NLRR-1* and *NLRR-3* genes, respectively. *Nbla10449/hNLRR-1* was preferentially expressed in UF NBLs, whereas *Nbla10677/hNLRR-3* was highly expressed in F NBLs (Fig. 3A).

Full-length cDNA cloning and structure of human NLRR-1, NLRR-2, NLRR-3 and NLRR-5 genes. We performed sequencing of whole inserts of *Nbla10449* and *Nbla10677* and defined their full-length cDNA sequences. In addition, during the process, we also identified human *NLRR-5* by homology search on the database. Furthermore, the other clone, *Nbla00061*, was found to be the same gene as *GAC1* which we renamed as h*NLRR-2*. *NLRR-4* has recently been reported by another group (15).

Nbla10449/hNLRR-1. A full-length *Nbla10449* genes comprised 3,060 bp, with an open reading frame (ORF) of 2,151 bp. The deduced protein was 716 a.a. in length, and included 2 hydrophobic stretches corresponding to a signal peptide at the extreme N-terminal region and a deduced transmembrane domain close to the C-terminal region (Fig. 1A). Analysis of the extracellular domain revealed the presence of 11 leucine-rich repeats encompassed by flanking cystein cluster, a leucine-rich repeat N-terminal domain (LRRNT) and a leucine-rich repeat C-terminal domain (LRRCT), a single immunogloblin C2 type domain, and a fibronectin type III domain (Fig. 1). Homology search against public database showed that *Nbla10449* was identical to the human *EST KIAA1497* (GenBank/DDBJ accession number AB040930) which lacked the N-terminal region and was similar to 2 leucine-rich repeat proteins, m*NLRR-1* (acc. no. D45913) and *Xenopus* x*NLRR-1* (acc. no. AB014462). The identities of deduced Nbla10449 protein to mNLRR-1 and xNLRR-1 were 92 and 75%, respectively. We also analyzed genomic structure of *Nbla10449*, and found that this gene comprised of single exon without any intron and mapped to chromosome 3p region.

Nbla10677/hNLRR-3. Nbla10677 comprised 2,471 bp with an ORF of 2,127bp (acc. no. AB060967) without intron, and mapped to chromosome 7q31. The deduced protein contained 708 a.a. and had a similar structure to Nbla10449/hNLRR-1 (Fig. 1A). In addition, the RGD sequence, an integrin-binding domain, was found in the leucine-rich repeats. Homology search showed that *Nbla10677* was identical to human cDNA FLJ11129 (acc. no. AK001991) and highly similar to the leucine-rich repeat proteins of mouse (mNLRR-3; acc. no. D49802) and rat (rNLRR-3; acc. no. AF291437). Therefore, Nbla10677 seemed to be a human NLRR-3. The Nbla10677/hNLRR-3 showed 85 and 83% similarity to mNLRR-3 and rNLRR-3 proteins, respectively.

Nbla00061/GAC1/hNLRR-2. The *Nbla00061* cDNA clone comprised 3,206 bp including a partial ORF of 2,142 bp. Sequence analysis revealed that it is identical to a *glioma amplified on chromosome 1* gene, *GAC1* (acc. no. AF030435), mapped to chromosome 1q32.1. The GAC1 protein, which was previously reported to be a member of an NLRR protein family (15), had 713 a.a. with a similar structure to NLRR-1 and 3 (Fig. 1). GAC1 showed 98% identity to mNLRR-2, although the latter was reported as only a partial sequence (16). It showed only 54 and 50% identities to mNLRR-1 and mNLRR-3, respectively, indicating that Nbla00061/GAC1 is a human counterpart of mNLRR-2.

m*NLRR-4* was cloned by another group from hemangioblast-like cell line derived from E11.5 mouse AGM and its predicted protein has 4 LRRs, fibronectin 3 and EGF-like motives in the extracellular region (Rump A *et al*, The Molecular Biology Society of Japan Conference, Yokohama,

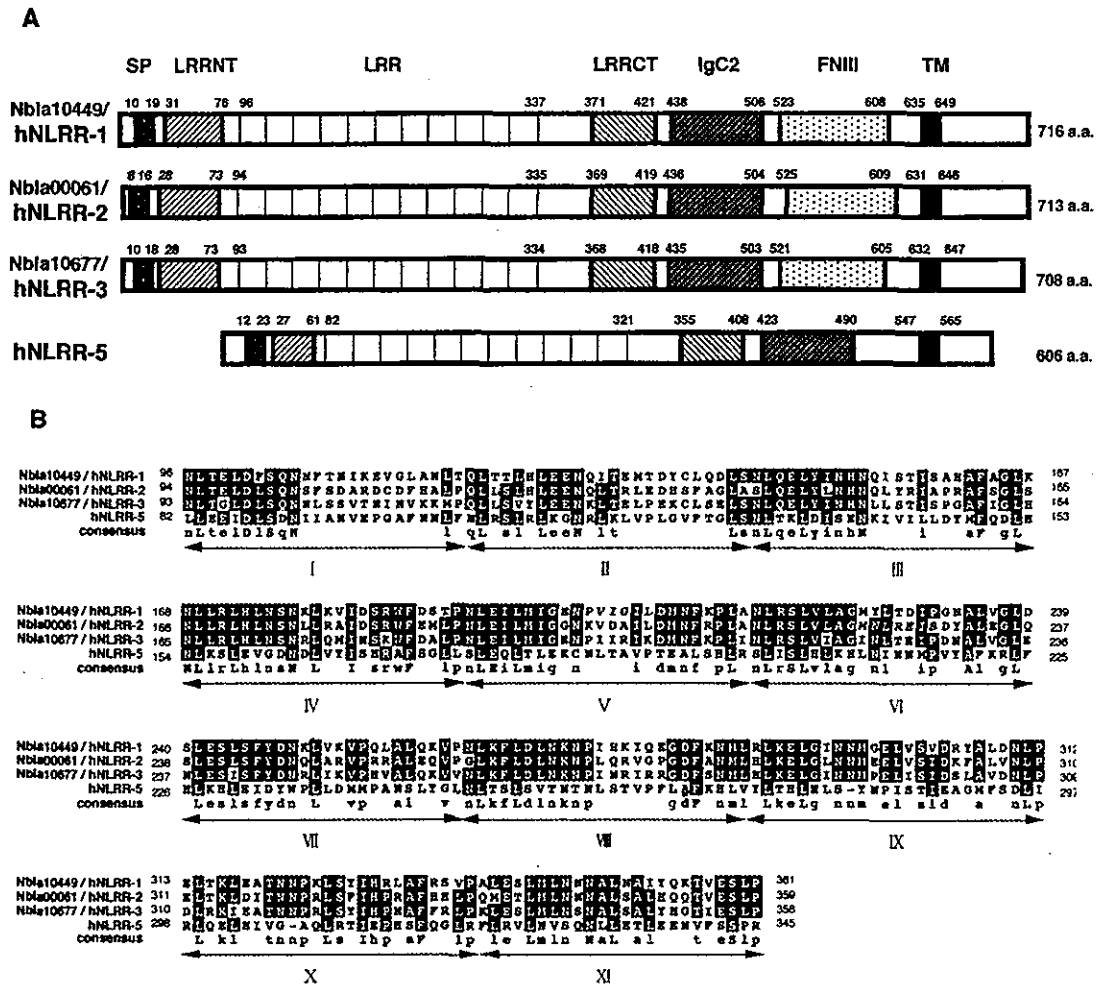

Figure 1. Structures and deduced amino acid sequences of hNLRR families. A, Schematic representation of hNLRR-1, hNLRR-2, hNLRR-3 and hNLRR-5 whose proteins consist of 716, 713, 708 and 606 a.a., respectively. SP, predicted signal peptide; TM, predicted transmembrane region; LRRNT, leucine-rich repeat N-terminal domain; LRRCT, leucine-rich repeat C-terminal domain; LRR, leucine-rich repeat; Igc2, immunoglobulin C-2 type domain; FN III, fibronectin type III domain. B, Amino acid alignment of the LRR domains of hNLRR families. Eleven repeats of LRR motif are shown by Roman numerals. Consensus sequences are highlighted and shown below.

abs. 4P-500 and 4P-501, 2001). h*NLRR-5* has no EGF-like motif and has 11 LRRs, and we failed to identify its human counterpart in the database or our NBL cDNA libraries.

h*NLRR-5*. Homology search against proteins deduced from genomic sequences on chromosome 9p revealed the presence of another family member of NLRR (acc. no. CAC22713). Its deduced protein was 606 a.a. in length and had a similar structure to the other NLRR members. However, a fibronectin domain was not included in this product. It showed 56 and 53% identities to mouse hypothetical protein (acc. no. BAB32403) and *Macaca fascicularis* hypothetical protein (acc. no. BAB03557), respectively, suggesting that they were mouse and *Macaca fascicularis* counterparts of hNLRR-5.

Expression of hNLRR family genes in human tissues. To examine whether *hNLRR* genes display neuron-specific expression, Northern analysis and semi-quantitative RT-PCR were performed. Among several human fetal tissues, h*NLRR-1*, h*NLRR-2* and h*NLRR-3* mRNAs were strongly expressed in brain at the size of 4.0-4.5 kb (Fig. 2A). By contrast, h*NLRR-5* was ubiquitously expressed in all main fetal organs. The size of h*NLRR-2* transcript in the liver was smaller than that in the other tissues. In adult human tissues, all h*NLRR-1*, h*NLRR-2*, h*NLRR-3* and h*NLRR-5* were also preferentially expressed at high levels in the nerve tissues (Fig. 2B).

Expression of hNLRR family genes in neuroblastoma and cell lines. Expression of h*NLRR* family genes was measured in primary neuroblastomas and cell lines using semi-quantitative RT-PCR. As shown in Fig 3A, *Nbla10449/hNLRR-1* was highly expressed in UF NBLs, whereas *Nbla10677/hNLRR-3* and h*NLRR-5* were preferentially expressed in the F NBLs. *Nbla00061/hNLRR-2* seemed to be equally expressed between both subsets. In NBL cell lines, expression of *NLRR-1* was observed relatively more frequently in the lines with *MYCN* amplification than in those with a single copy of the gene. On the other hand, *NLRR-3* appeared to be expressed rather frequently in the cell lines without *MYCN* amplification. Interestingly, however, there was a tendency that the cells with high expression of *NLRR-1* also had a high levels of expression of *NLRR-3* (Fig. 3B). The expression of both h*NLRR-2* and h*NLRR-5* was found in most NBL cell lines.

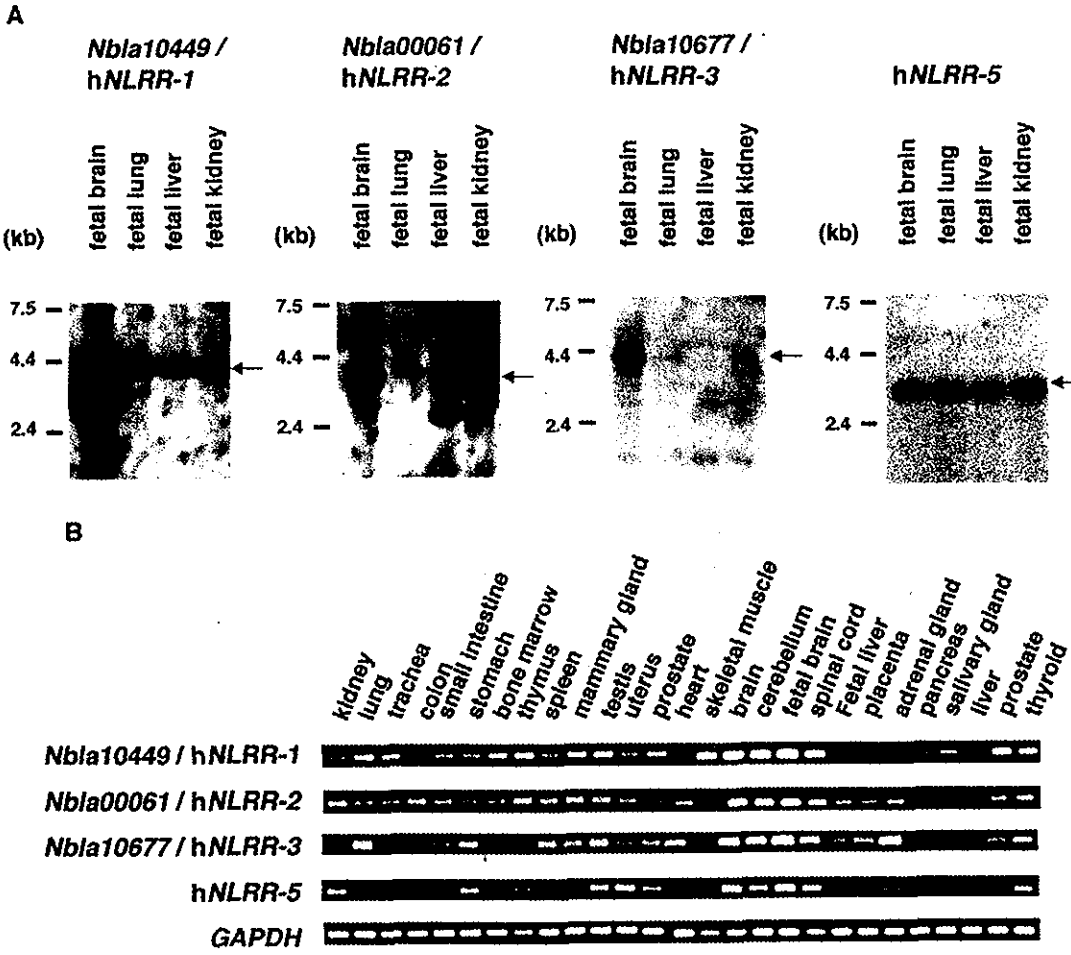

Figure 2. Expression of h*NLRR*s mRNA in human normal tissues. A, Northern blot analysis of h*NLRR*s mRNA in human fetal tissues. As a control for the amount of RNA, the same filter was rehybridized with ß-actin. B, Semi-quantitative RT-PCR of h*NLRR*s in multiple human tissues. Total RNA of 25 adult and 2 fetal tissues. As a control, same cDNA templates were amplified by *GAPDH* primers.

We then examined whether or not there was any genomic amplification of h*NLRR-1* or h*NLRR*-2 because that of *Nbla10449/hNLRR-1* was preferentially expressed in UF NBLs, and that of *GAC1/hNLRR-2* was reported to be amplified in the primary glioblastoma and anaplastic astrocytoma (15). However, our Southern blot analysis showed that neither of both genes was amplified in NBL cell lines so far examined (CHP134, IMR32, NB-9, NLF, TGW, NGP, NB69, NBL-S, SK-N-AS and SH-SY5Y) (data not shown). As regards the other cancer cell lines, expression of h*NLRR* family members was relatively restricted to the osteosarcoma and rhabdomyosarcoma cell lines (Fig. 3C). The low levels of h*NLRR*-3 and h*NLRR-5* expression were also seen in melanoma cell lines. Furthermore, expression of h*NLRR-2* was observed in the cell lines of colon, thyroid (medullary thyroid cancer), esophagus and lung. These results suggested that h*NLRR*s were preferentially expressed in the cell lines derived from neural crest cells.

Changes in expression of the NLRR family genes during NGF-induced differentiation and NGF-depletion-induced apoptosis in newborn mouse SCG neurons in primary culture. To investigate the role of NLRR family molecules in NGF/TrkA-mediated signaling, we next used newborn mouse SCG neurons, from which NBL is derived. As reported previously, NGF induced marked morphological differentiation of SCG neurons (14). NGF-induced neurite extension was observed on day 2 and was enhanced thereafter by increasing in number and length (Fig. 4A, NGF$^+$). The depletion of NGF by treating the cells with anti-NGF antibody induced neuronal programmed cell death (Fig. 4A, NGF$^-$). As shown in Fig. 4B, expression of m*NLRR-1* and m*NLRR-5* was down-regulated during NGF-induced neuronal differentiation, and was up-regulated after NGF deprivation (Fig. 4B). On the other hand, expression of m*NLRR-2* and m*NLRR-3* was slightly up-regulated when they were treated with NGF, and was significantly down-regulated after NGF deprivation (Fig. 4B), suggesting that expression of m*NLRR* genes might be related to the NGF signaling.

Prognostic significance of expression of Nbla10449/hNLRR-1 and Nbla10677/hNLRR-3 in primary neuroblastomas. To evaluate the clinical significance, expression of *Nbla10449/* h*NLRR-1* and *Nbla10677/*h*NLRR-3* in 99 NBLs was statistically analyzed. Table I gives the mean and standard error (SEM) of h*NLRR-1/Nbla10449* and h*NLRR-3/Nbla10677*